Universidade de São Paulo

Instituto de Física de São Carlos

Luiz Eduardo Raphael da Rocha

Platinum micromachining using femtosecond laser pulses

São Carlos
2023

Luiz Eduardo Raphael da Rocha

Platinum micromachining using femtosecond laser pulses

Dissertation presented to the Graduate Program in Physics at the Instituto de Física de São Carlos, Universidade de São Paulo to obtain the degree of Master of Science.

Concentration Area: Theoretical and Experimental Physics

Advisor: Prof. Dr. Cleber Renato Mendonça

Original version

São Carlos
2023

Rocha, Luiz Eduardo Raphael da
Platinum micromachining using femtosecond laser pulses / Luiz Eduardo Raphael da Rocha; advisor Cleber Renato Mendonça -- São Carlos 2023.
68 p.

Dissertation (Master's degree - Graduate Program in Theoretical and Experimental Physics) -- Instituto de Física de São Carlos, Universidade de São Paulo - Brasil , 2023.

1. Femtosecond micromachining. 2. Non linear optics. 3. Platinum micromachining. 4. Incubation effect. 5. Laser induced forward transfer. I. Mendonça, Cleber Renato, advisor. II. Title.

FOLHA DE APROVAÇÃO

Luiz Eduardo Raphael da Rocha

Dissertação apresentada ao Instituto de Física de São Carlos da Universidade de São Paulo para obtenção do título de Mestre em Ciências. Área de Concentração: Física Teórica e Experimental.

Aprovado (a) em: 29/08/2023

Comissão Julgadora

Dr(a).: Cleber Renato Mendonça

Instituição: (IFSC/USP)

Dr(a).: Gustavo Foresto Brito de Almeida

Instituição: (UFU/Uberlândia)

Dr(a).: Jonathas de Paula Siqueira

Instituição: (UNICAMP/Campinas)

"Dedicated to my family and friends, who gave me love and support."

Acknowledgments

Firstly, I would like to thank my advisor, Prof. Dr Cleber Renato Mendonça, who gave all the support I needed during my Master's degree, and also during my undergraduate years, for the project that started my academic experience and the advices in the classes I took.

I would like to thank my collegues and friends of the Photonics Group at IFSC, current and former members, for all the help they gave me and the shared experiences, as well as Prof. Dr. Leonardo de Boni and Prof. Dr. Lino Misoguti, who all were always open to help in the laboratory and create a positive and collaborative atmosphere.

Thanks to the Photonics Group staff, Daniel Pereira, for the great job and help with burocratic matters and André Romero for the alwesome technical help, learnings and dedication in the group's laboratories.

I would like deeply thank my best friends, André Pelosi and Kauê Curvelo, for all the amazing work hours together, helping many moments to be lighter, and for all the emotional support given during the undergraduate and Master's years, they both were always by my side during the most difficult moments I had. And of course, for the friendship I got for my life.

I would like to express my gratitude to my parents, Lilian and Irano Rocha, as well as my sister Beatriz Rocha, for the support in all my choices and paths I took, and for the unconditional love they gave me.

Lastly, I would like to thank for all the financial support gave by CAPES and FAPESP, and all the Physics Institute of São Carlos staff, always able to help.

“Science is the poetry of reality” – Richard Dawkins

THIS STUDY WAS FINANCED IN PART BY THE COORDENAÇÃO DE APERFEIÇOAMENTO DE PESSOAL DE NÍVEL SUPERIOR - BRASIL (CAPES) - FINANCE CODE 001.

ABSTRACT

ROCHA, L. E. R. **Platinum micromachining using femtosecond laser pulses.** 2023. 68 p. Dissertation (Master of Science) – Instituto de Física de São Carlos, Universidade de São Paulo, São Carlos, 2023.

Among the many techniques for micromachining, the Direct Laser Writing (DLW) introduces some advantages to the process, such as high resolution, size, and thickness control, while maintaining the materials proprieties after the procedure. The Laser Induced Forward Transfer (LIFT) is a DLW technique, whose principle is to transfer energy from the laser pulse to the sample, ejecting material droplets from the region where the laser beam is focalized. The technique can be performed using ultrashort laser pulses, which leads to nonlinear light-matter interaction, enabling high-resolution depositions and avoiding degradation of the transferred material. A variety of materials can be studied with LIFT, including metals, which draw attention due to its applications. Platinum micromachined structures are used to produce sensors, because of the material stability in different conditions and other applications. In this work, thin films of platinum (Pt) have been used as donor material for fs-LIFT. To characterize the deposition of Pt on glass, optical microscopy and scanning-electron microscope were used. Besides, the influence of the pulse repetition rate, pulse energy, and scanning speed on the produced features was investigated to determine the optimum irradiation parameters, as well as the threshold fluence. The incubation effect, the thickness control by the repetition rate and the production of different structures were studied. The depositions were made using two laser systems, one centered at 800 nm (5 MHz and pulse energy of nJ), and another one centered at 1030 nm (1 to 1000 kHz and pulse energy of µJ). It was observed that the optimum parameters are achieved with energies from 3 to 6 µJ and repetition rate around 1 kHz, as the depositions get homogeneous and well-defined, as well as the possibilities of micromachining tri-dimensional structures and different kind of depositions varying the micromachining conditions.

Keywords: Femtosecond micromachining. Non linear optics. Platinum micromachining. Incubation effect. Laser induced forward transfer.

RESUMO

ROCHA, L. E. R. **Microfabricação de platina usando laser de pulses de femtosegundos.** 2023. 68p. Dissertação (Mestrado em Ciências) – Instituto de Física de São Carlos, Universidade de São Paulo, São Carlos, 2023.

Dentre as muitos técnicas de microfabricação, as técnicas de Escrita Direta a Laser, ou "Direct Laser Writing" (DLW), trazem grandes vantagens ao processo, como a alta resolução, o controle do tamanho e da espessura na microfabricação e mantendo as propriedades do material após o procedimento. A técnica de Transferência Induzida a Laser, ou Laser Induced Forward Transfer (LIFT), é uma técnica de Escrita Direta a Laser em que seu princípio é transferir a energia de um pulso do laser para uma amostra, fazendo com que o material que absorve a energia na região em que se focalize o feixe seja transferido em gotas para um substrato. A técnica pode ser usada associada a um laser de pulsos ultracurtos, o que gera uma interação não linear da luz com a matéria, e com isso, a técnica resulta em deposições de alta resolução e qualidade e evitando a degradação do material transferido. Uma grande variedade de materiais podem ser estudados via LIFT, incluindo metais, que chamam atenção dos pesquisadores por suas aplicações tecnológicas. Estruturas microfabricadas de platina são usadas para produção de sensores, principalmente, por sua alta estabilidade em diferentes condições, além de outras aplicações. Neste trabalho, filmes finos de platina (Pt) foram usadas como doadoras de material para a técnica de LIFT com femtossegundo. Para caracterizar as microfabricações de platina em lâminas de vidro,, microscopia óptica e microscopia eletrônica de varredura foram usadas. Além disso, foi estudada a influência da taxa de repetição do laser, a energia do pulso e da velocidade de varredura na microfabricação, e determinadas as melhores condições de microfabricação da platina nos setups usados, além de determinar a fluência de threshold e estudar o efeito de incubação. Dois sistemas foram usados, um centrado em 800 nm (5 MHz e energias em nJ) e outro centrado em 1030 nm (1 kHz à 1 MHz e energias em µJ). Foi observado que as melhores condições de microfabricação são no segundo sistema, com energias de 3 à 6 µJ, taxa de repetição próxima a 1 kHz, além de que as deposições são homogêneas e bem definidas. Além disso, foram estudadas diversas estruturas e mostrada a possibilidade de fazer microfabricação de estruturas tri-dimensionais.

Palavras-chave: Microfabricação com laser de femtossegundos. Óptica não linear. Microfabricação de platina. Efeito de incubação. Transferência induzida a Laser.

LIST OF FIGURES

LIST OF ABREVIATIONS AND ACRONYMS

fs	femtosecond
DLW	Direct Laser Writing
LIFT	Laser Induced Forward Transfer
Pt	Platinum
NP	Nanoparticle
PtNP	Platinum Nanoparticle
SHG	Second harmonic generation
THG	Third harmonic generation
CPA	Chirped-Pulse Amplification
NA	Numerical aperture
SEM	Scanning Electron Microscopy
IFSC	Instituto de Física de São Carlos
USP	Universidade de São Paulo

LIST OF SYMBOLS

E_g	Energy gap
ν	Frequency
h	Plank's constant
γ_k	Keldysh parameter
F_{th}	Threshold fluence
c	Speed of light
L	Laser Cavity length
I	Laser Intensity
h	Plank’s constant
e	Electron charge
r_{th}	Threshold radius
w_0	Gaussian beam waist at the focus
E_p	Pulse energy
E_{th}	Threshold energy
f	Pulsed laser repetition rate
N	Pulse superposition number
V	Scanning speed
λ	Wavelength of light
k	Incubation parameter
$F_{th,N}$	Threshold fluence of N pulses

CONTENTS

1 INTRODUCTION

The laser was first demonstrated by Theodore H. Maiman in 1960 (1), and it became a fundamental tool for many applications in science and technology. One of the many laser applications is material processing, which became even more interesting when ultrashort laser pulses emerged, opening new opportunities in this area. Using laser pulses with a duration of hundreds, or even tens, of 10^{-15} seconds (femtosecond), permits material's processing with much less heat-affected zone outside the irradiated spot became available, giving rise to the so-called femtosecond (fs) laser micromachining. (2) This regime proved to have advantages over the one with longer pulses, since it allows producing micro/nanostructures with a higher resolution. (3) Researchers have already related fs-laser micromachining characteristics to nonlinear phenomena, which take place during the process due to its high energies.

The material deposition in micro/nanoscale has many applications, from optical and photonic devices to microelectronics. (4-6) The need for micro/nanoscale technologies is now strong, starting with microelectronics a few decades ago, it has spread to other areas, such as telecommunications, medicine, and many more research and industry areas. (7-8) Many techniques using pulsed lasers have been developed for micromachine devices, and Direct Laser Writing (DLW) is among them. Those DLW techniques have some advantages, such as it doesn't rely on complex or expensive systems, high resolution, control of several fabrication parameters, fast processing, and maintaining the material properties after the process.

The Laser Induced Forward Transfer (LIFT) technique use has grown in the past few years, and one of the reasons for that is the technique's ability to deposit a wide variety of materials, such as metals (9-10), polymers (11), semiconductors (12), two-dimensional materials (13) and biomaterials (14), and in different kinds of substrates. Because of the nonlinear light-matter interaction nature, using LIFT with ultrashort pulsed lasers results in a high-resolution deposition. Also, because thermal effects are minimized using an ultrashort pulsed laser, the material keeps its characteristics after the process. (15-16) LIFT's principle is to irradiate the backside of a donor substrate, which contains the material (thin film) on one side, transferring it to the receiving substrate, placed right below the donor. The donor-receiver system can be in contact or not. The technique doesn't require any special ambient conditions to be carried out, nor any sample treatment before the process. Those cited characteristics make LIFT one of the most versatile micromachining techniques created until now.

One of the most common ways to produce nanoparticles (NPs) is through an aqueous solution, first observed in the 20th century (17), which consists of reducing noble metals

producing NPs. Another method is heating and cooling the material in ceramic ovens(18), which usually takes too much time and uses too much energy. With the development of the LIFT, it became one major alternative to produce metallic NPs, due to its parameters control, which leads to the NPs size and shape control. Metallic NPs and their macrostructures have physical, chemical, and biological differences due to the high surface-volume ratio. (19) Platinum nanoparticles (PtNPs) have interesting chemical and physical properties that make them applicable to several research areas. PtNPs are free electron metal NPs, and just like silver and gold, their optical response is dictated by the surface plasmon resonance (SPR). SPR is the resonant oscillation of conductive electrons on the surface of a material irradiated by incident light. SPR of PtNPs is mostly found at 215 nm (UV). (20) The stability of PtNPs is the reason for efficient membrane fuel cells development. (21-22) Also, PtNPs can be used in the electronics industry, manufacturing conductive film circuits and internal electrodes of multilayer capacitors. (23)

Platinum (Pt) has been used for centuries by ancient Chinese, Egyptians, and pre-Colombians for jewelry and decorations (a moldable and shiny material). Still, the first European scientific report of it appeared in 1557 by the Italian scientist *Julius Caesar Scalinger*, in Mexico. This "new" material, *platinum*, was named in reference to the word *Plata* which means *silver* in Spanish. It has been described as an unknown metal "*which no fire nor any Spanish artifice has yet been able to liquefy*", which was first thought to be an impurity. (24) Platinum is a very rare metal (0,005 ppm in Earth's crust (25) - one of the reasons for its elevated price), being most mined in South Africa (around 80% of the world's total production). Just a few hundred tons are produced annually (in comparison, for gold, it is a few thousand). Platinum is one of the least reactive metals and has a great resistance to corrosion even in high temperatures, and therefore it was considered a noble metal. A Pt bar was used until 2019 as the kilogram definition since 1879 and used as a meter standard from 1889 to 1960. (26) Platinum has applications in a variety of research areas, from medicine to modern technology. For example, it has often been used in chemical compositions of tumoral medicines. (27) Also, modern fuel cells with Pt were found to cause less ambiental damage (28) and to enhance the efficiency of solar cells.(29) In the micromachining field, platinum has also been used, for example, in biosensors (30) and thermal microsensors. (31)

In this dissertation, we studied the femtosecond-LIFT process of platinum. Using the zero damage method (32) and analyzing the influence of the number of pulses on the LIFT process (incubation effect), the best deposition conditions were determined. Upon such characterization, different structures were microfabricated, such as tri-dimensional structures

and split-ring resonators. The further chapters of this dissertation will treat the fundamental theories behind the experimental process (Chapter II), the experimental setup (Chapter III), the results (Chapter IV), and conclusions of this study (Chapter V).

2 FUNDAMENTALS

Chapter II addresses the theoretical basis to understand the results discussions presented in this dissertation, covering aspects of light-matter interaction (nonlinear optics and nonlinear absorption), femtosecond laser micromachining, and the micromachining technique used in this work, Laser-Induced Forward Transfer (LIFT).

a) Nonlinear Optics

Nonlinear optics is the study of light-matter interaction in the regime in which the light itself modifies the proprieties of the material . (33) Nonlinear optical regimes can be achieved when the light source has enough intensity to induce such effects. After Franken *et al*. (34) demonstrated the second harmonic generation in 1961, the research for nonlinear materials that could be used in optical and photonic devices was intensified.

Ultrashort laser pulses have an extremely high peak intensity, as discussed in the next section, leading to an electric field amplitude of about the same order of magnitude as the interatomic electric field, leading to a nonlinear light-mater interaction. (32) The induced polarization in linear optics can be described by

$$\vec{P}(t) = \varepsilon_0 \chi^{(1)} \vec{E}(t), \tag{2.1}$$

where ε_0 is the vacuum permittivity and $\chi^{(1)}$ is the linear susceptibility. Equation 2.1 should be modified to work in nonlinear optics, as the model of the atom treated as a harmonic oscillator is not adequate anymore. In this case, the atom must be treated as an anharmonic oscillator, indicating that Eq. 2.1 should be expressed as a power series, as

$$\vec{P}(t) = \varepsilon_0 \left[\chi^{(1)} \vec{E}(t) + \chi^{(2)} \vec{E}^2(t) + \chi^{(3)} \vec{E}^3(t) + \cdots \right], \tag{2.2}$$

where $\chi^{(2)}$ and $\chi^{(3)}$ are second and third-order nonlinear optical susceptibilities. The first term recalls Eq. 2.1, representing matter's linear response, whilst the other terms represent the nonlinear response, as the induced polarization depends nonlinearly on the electric field. Therefore, Eq. 2.2 can be rewritten as the sum of the linear and nonlinear responses, such as

(2.3)

$$\vec{P}(t) = \overrightarrow{P_L} + \overrightarrow{P_{NL}}$$

As it can be seen, linear optics is treated as a particular case of nonlinear optics. Each term of the nonlinear response can be associated with different nonlinear phenomena. Second-order susceptibility is responsible for second harmonic generation (SHG) and optical ratification, e.g.. The third-order term is responsible for third harmonic generation (THG) and optical Kerr effect, and so on. Considering a third-order nonlinear optical process and a monochromatic electrical field given by

$$E(t) = E_0 \cos(\omega t), \tag{2.4}$$

the third-order term in Eq. 2.2 can be written as

$$\vec{P}^{(3)}(t) = \frac{1}{4}\varepsilon_0 \chi^{(3)} E_0^3 \cos(3\omega t) + \frac{3}{4}\varepsilon_0 \chi^{(3)} E_0^3 \cos(\omega t). \tag{2.5}$$

The first term in Eq. 2.5 refers to the THG, as for a field applied with frequency ω there is a response of 3ω.(33) The second term refers to a nonlinear behavior at the same optical field frequency as the polarization, leading to a nonlinear change in the refractive index, at frequency ω, with the light intensity. Thus, the refractive index can be written as

$$n = n_0 + n_2 I, \text{ as } I = \frac{1}{2} n_0 \varepsilon_0 c E_0^2, \tag{2.6}$$

where n_0 is the linear refractive index, I is the incident field intensity and n_2 is the nonlinear refractive index, described as

$$n_2 = \frac{3}{2 n_0^2 \varepsilon_0 c} \chi^{(3)}. \tag{2.7}$$

Equation 2.7 refers to the Optical Kerr effect, which describes the refractive index as dependent on the incident field intensity.

b) Nonlinear Absorption

Linear absorption is the process in which the material absorbs enough energy from a photon that the electrons in the valence band (highest occupied energy level) are promoted to the conducting band (lowest unoccupied energy level). The valence and conducting bands are separated by a potential barrier with an energy gap (E_g). The material can absorb an incident photon with energy greater than E_g, promoting the electrons in valence band to the conducting band;

$$h\nu > E_g, \tag{2.8}$$

where h is Plank's constant and ν the incident field frequency.

If a single photon doesn't have enough energy ($h\nu < E_g$), the only way to excite the valence band electrons is through nonlinear absorption processes, which are photoionization and avalanche ionization[35], in which the first one can be split into tunneling and multiphotonic ionization.

In a high-intensity and low-frequency system, the electromagnetic field is sufficiently intense to distort the band's structure, reducing the potential barrier between valence and conducting band (Fig. 1a). This way, the electrons can be promoted to the conducting band by quantum tunneling.

Multiphotonic ionization (Fig. 1b) is a process associated with the imaginary part of the nonlinear susceptibility.(33) In this case, multiple (m) photons are absorbed at the same time by a single electron in valence band, in which $mh\nu > E_g$.

Keldysh(36) demonstrated that both processes are the same, only distinguished by the frequency regime (low or high frequency). This can be determined by the electron tunneling time as compared to the field period, which is the Keldysh parameter (γ_k), written as

$$\gamma_k = \frac{\nu}{e}\sqrt{\frac{m_e \varepsilon_0 c n_0 E_g}{I_0}}, \tag{2.9}$$

where ν is the field frequency, e and m_e are the electron's charge and mass, c the light speed, and I_0 the field intensity. If γ_k"1, it is a low-frequency regime, with tunneling being the dominant process. If γ_k"1, it is a high-frequency regime, and the electron oscillates so fast that the band distortion isn't perceived, and the multiphotonic ionization is dominant.

The avalanche ionization (Fig. 1c) occurs when an electron in the conduction band ("seed" electron) absorbs energy greater than E_g. In this case, the seed electron, colliding with a valence electron (impact ionization), would ionize it, giving rise to two electrons in the lower conduction band. While the incident field is present, this process continues, exponentially growing the electron density in the conduction band (avalanche ionization), and a plasma is created in the material.(35) The seed electron needed to start the avalanche ionization is usually previously originated by tunneling or multiphoton ionization.

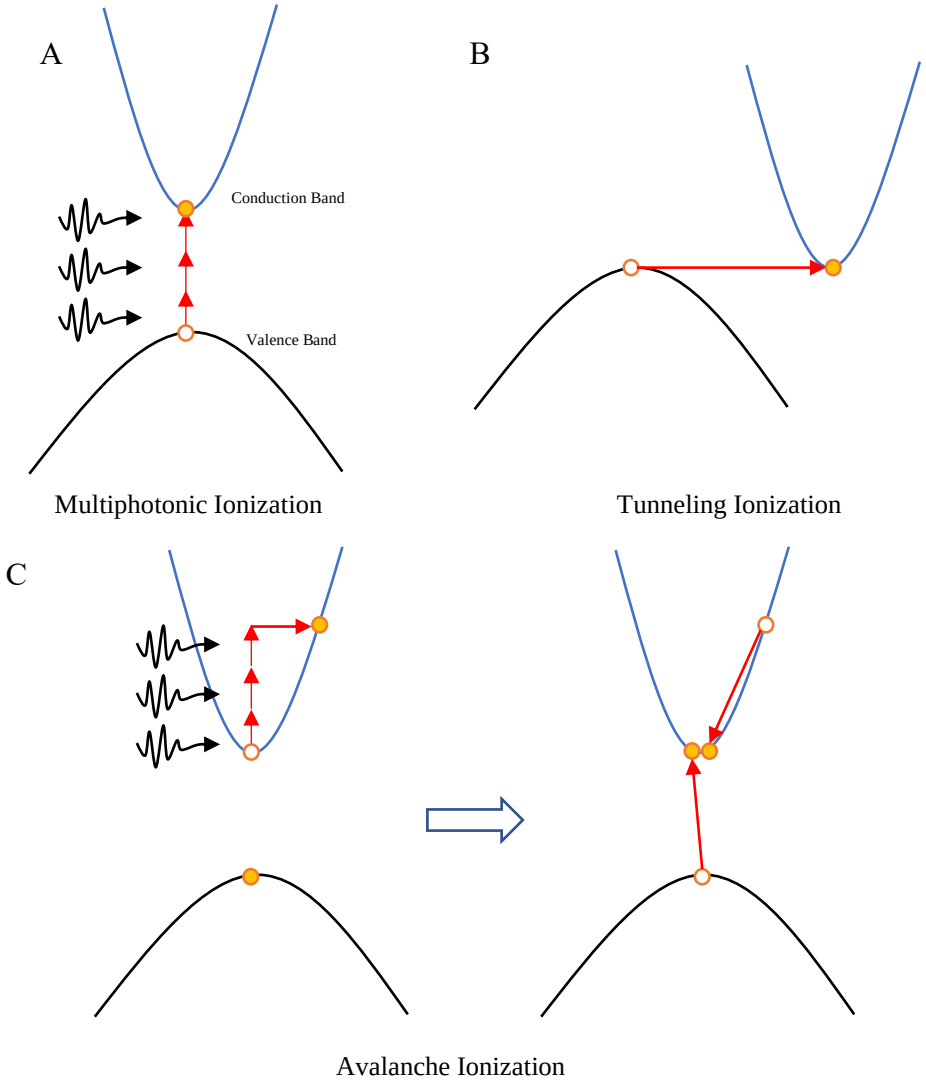

Figure 10 - Nonlinear photoionization by a) tunneling, b) multiphotonic ionization and c) avalanche ionization.

*Source: Adapted from AMS.(*35)

c) Ultrashort Laser Pulses

Ultrashort laser pulses are those pulsed lasers with temporal width ranging from picoseconds (10^{-12} s) to femtoseconds (10^{-15} s), and it has a broadband spectrum and high peak power. The generation of this kind of laser pulses requires a specially designed cavity, composed of mirrors, lenses, and dispersion compensation elements (such as prisms, since different components of light tend to despair, once each have different frequencies and, therefore, travel in different speeds). It also requires a wide emission spectrum gain medium excited by a pump source and, finally, a mode-locking mechanism.(37)

The cavity geometry and the gain medium are fundamental to the laser output spectrum, as they act as special filters. Not all frequencies can resonate in the cavity, only those with an accumulated phase of an integer multiple of 2π over a round trip. Those frequencies ($m2\pi$) will constructively interfere, forming oscillating stationary waves, and the other frequencies will destructively interfere, annihilating them. Following this, the resonant frequencies that compose the laser output with a cavity length L are

$$\nu_m = m\frac{c}{2L} \tag{2.10}$$

where m is a positive integer. It's intrinsic in Eq. 2.10 that an infinite number of frequencies are allowed to resonate in the cavity. However, the gain medium selects which ones will be excited, due to its continuum-wide spectrum emitted, containing cavity resonant frequencies that oscillates. This situation is illustrated in Fig. 2. Figure 2a indicates the infinite number of frequencies allowed to oscillate by the cavity; Fig. 2b represents the wide spectrum emitted in the gain medium. Finally, Fig 2c shows the actual excited modes allowed by the gain medium. The number of oscillating modes in the cavity is very high, and the gain medium material plays an important role. One of the most popular ones is the Ti:Sapphire crystal, due to its thermal and optical proprieties, with a wide absorption spectrum centered at approximately 500 nm and a very wide emission spectrum (from 700 nm up to 1000 nm, centered at 790 nm).(38) Considering a cavity length of 1 meter, more than 9 x 10^5 modes can oscillate in the cavity.

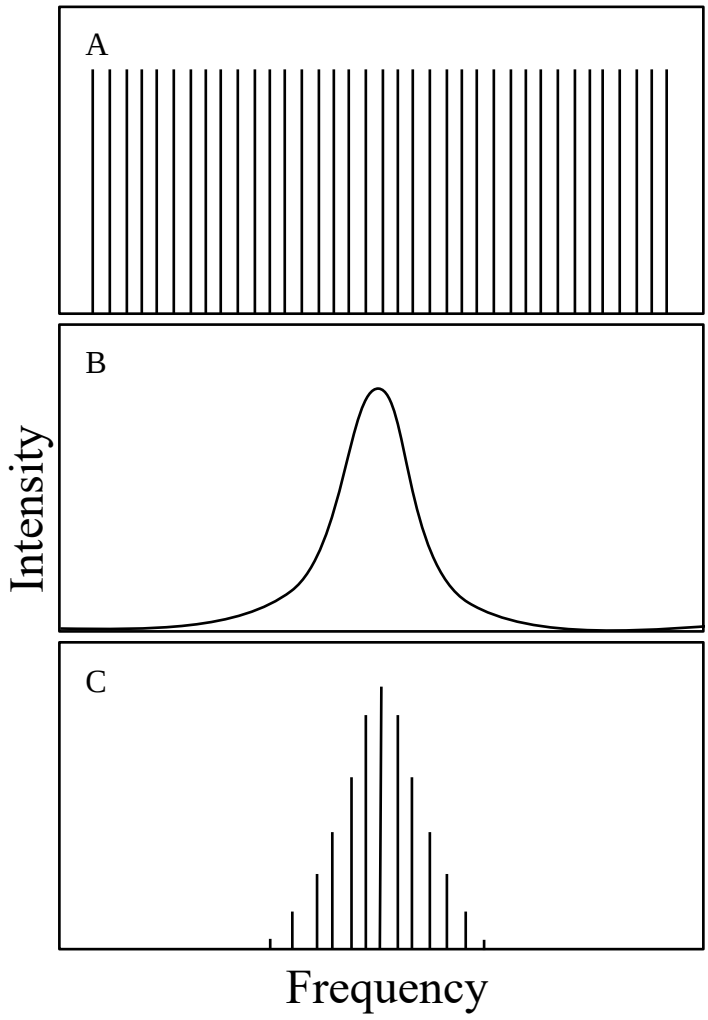

Figure 11 – Schematic representation of a) the infinite modes allowed to oscillate by the cavity, b) the gain medium spectrum and c) the actual allowed frequencies.

Source: By the author.

In a highly excited cavity, the sum of all propagating fields gives the laser output, as

$$E(t) = \sum_{m=1}^{N} E_m exp\{-i(2\pi\nu_m t + \phi_m)\} \tag{2.11}$$

where *N* is the total number of excited modes with frequency ν_m, amplitude E_m and phase ϕ_m. There must be a controlling mechanism applied, as the laser output tends to be unstable due to the high number of electric fields in the cavity. Ultrashort pulses are generated when the phase of the modes are locked with each other. (39) The mode-locking mechanism organizes the modes by making the relative phases between them constant ($\phi_m = constant$). This creates constructive interference, resulting in an extremely high and intense short pulse. As it can be

seen in Fig. 3, when the number of modes increases, each pulse gets more intense and shorter, achieving the ultrashort range.

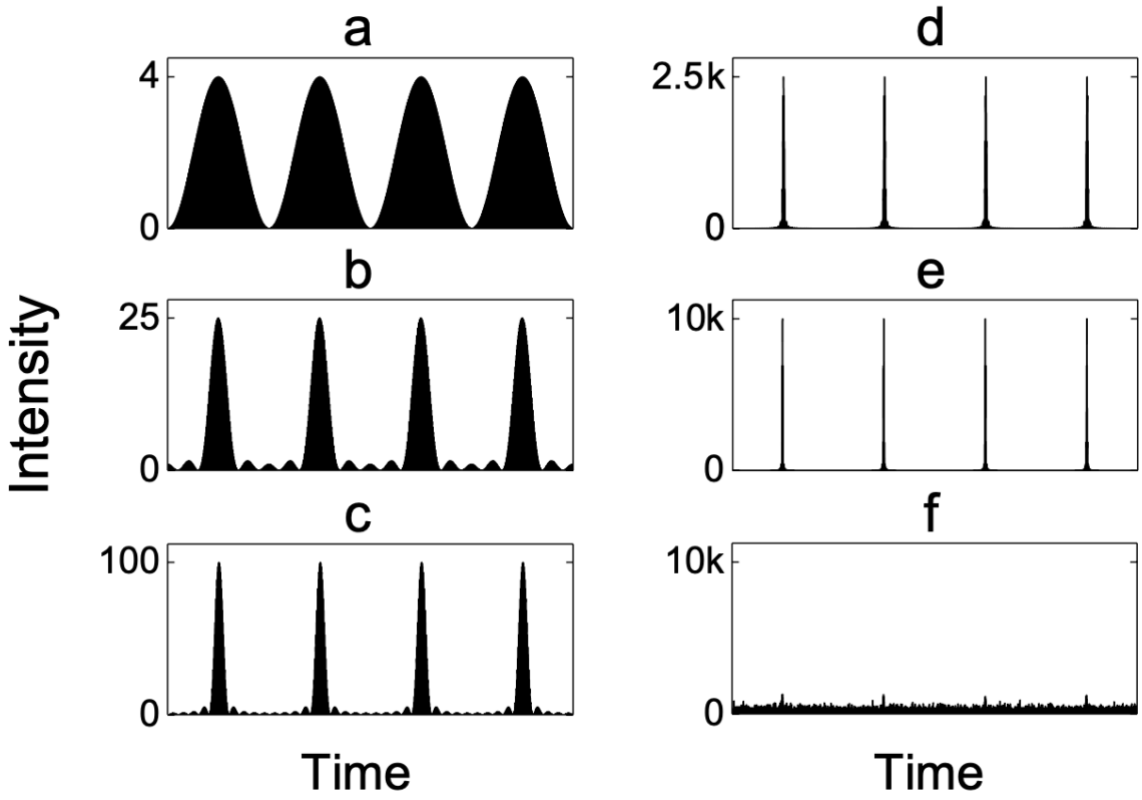

Figure 12 – Laser output intensity in function of time in mode-locking regime with a) 2, b) 5, c) 10, d) 50, e) 100 modes and f) 100 modes with random relative phases.

Source: ALMEIDA. (40)

There are systems capable of increasing the pulse energy by some orders of magnitude, called amplified laser systems. Still, for femtosecond laser pulses, it should be done with care, as the energy can get so high that it damages the optical elements inside the cavity. The Chirped-Pulse Amplification (CPA)(33) is a technique used to avoid this damage situation. CPA stretches a low-energy pulse temporally by diffraction gratings, so its peak intensity is insufficient to cause any damage in the cavity. After this, the amplificated pulse is compressed by a pair of diffraction gratings, generating a more intense ultrashort pulse. The CPA system is illustrated in Fig. 4.

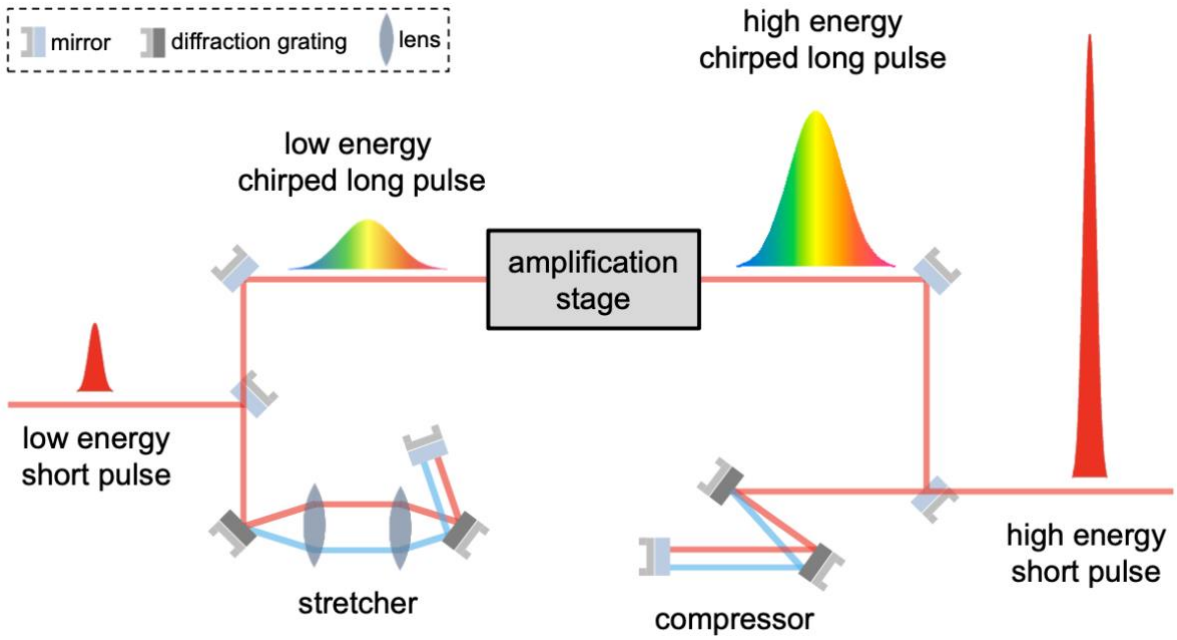

Figure 13 – Illustration of a CPA system.

Source: ALMEIDA. (40)

d) Femtosecond Laser Micromachining

Femtosecond laser micromachining is one of the processes used to produce micro-sized structures inside the bulk or surface of a solid material with precision. The technique relies on the process discussed in Sections 2a and 2b, as the femtosecond laser has such an intense and short pulse (Section 2c), it can induce nonlinear ionization in its focal volume, ionizing a density of electrons, which transfer such energy to the lattice, generating a plasma, causing the optical breakdown and, therefore, causing permanent damage. The optical breakdown process has been studied for a long time, as Hercher *et al.* (41) reported back in 1964. In 1995 the first paper on the use of femtosecond laser micromachining was published (42), promoting the technique and unclogging it for other advances to appear.

The feature produced depends strongly on many experimental parameters, such as pulse energy and duration, repetition rate, wavelength, scanning speed, and objective numerical aperture, for instance. They also depend on the material's optical and thermal properties.

Micromachining associated with ultrashort laser pulses carries some advantages compared to other methods. Firstly, the unwanted thermal damage in the lattice is reduced. This happens with an ultrashort (picosecond or femtosecond) pulse because the pulse duration is

shorter than the energy dissipation around the focal volume (up to nanosecond). The pulse energy is absorbed just by the material's electrons. After that, the accumulated energy is transferred to the ions and starts the thermalization process after the pulse has left the material. In this situation, the lattice and electronic systems can be treated separately, and the damage is confined. This process is called the two-temperature model. (43) Figure 5 illustrates the difference in micromachining between a long (a) and ultrashort (b) laser pulse. The second reason is due to the nonlinear absorption, since it governs the micromachining process.

When the electron density reaches a certain point, it transfers its energy to the lattice, suddenly increasing its temperature and, therefore, removing material from the area. (44-45) At the same time, the avalanche ionization occurs, leading to a Coulomb explosion, as the charge in the surface gets unbalanced.

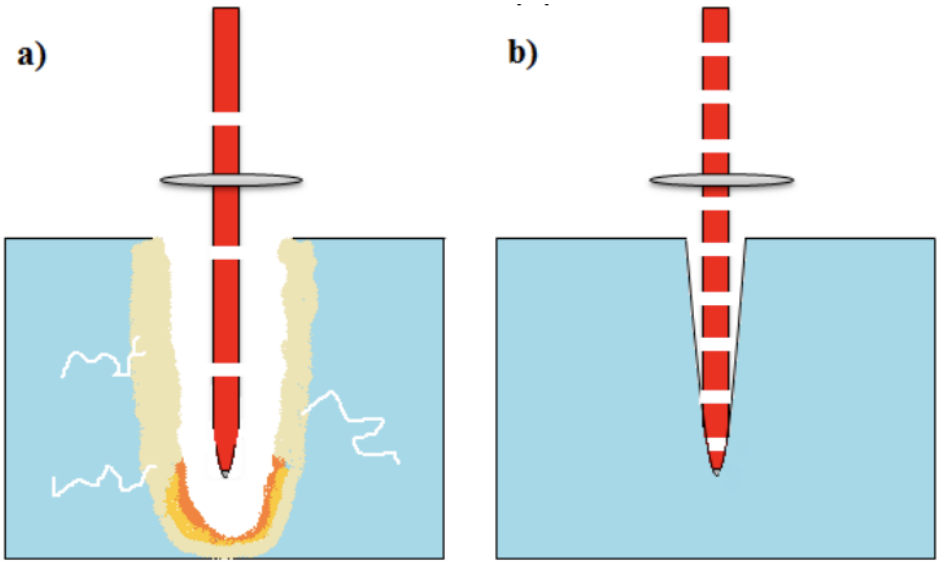

Figure 14 – Difference between micromachining with a a) long pulse and b) an ultrashort pulse.

Source: Adapted from NOLASCO. (46)

To optimize the micromachining process it is important to know the minimum applied energy per area to do damage , which is called the threshold fluence (F_{th}). Knowing such parameter can help to produce better structures and reduce unwanted damage around the area. This value can change due to various aspects, like impurities and defects in the material's composition. (47) The threshold fluence decreases if the number of pulses per spot of the material increases; this is called the incubation effect. (48) In chapter III the incubation effect calculations will be better described.

e) Laser-Induced Forward Transfer

Laser Induced Forward Transfer (LIFT) is a micromachining technique that consists in transferring material from a donor to a receiver substrate, and it was demonstrated by Bohandy(49), in 1986, transferring copper to a silica substrate. In 1987, LIFT's mechanism and numerical model were published. (50) After that, many LIFT variations were developed and used for many materials(51-53), with several applications in metals (54-58), making it one of the most versatile DLW techniques.

LIFT is a high-resolution direct-write technique. A thin film of a target material (donor) coated in a transparent material (carrier) is placed near or in contact with a substrate (receiver). When a laser beam is focalized onto the donor/receiver interface, it starts the ablation process discussed in previous sections, depositing material in the receiver substrate. When the donor/receiver substrate is placed above a moving stage, the technique can be used to do complex structures with high resolution.

Depending on the experimental conditions, the donor can be melted or partially vaporized. Due to the thermally induced stresses (59-60) and the rising pressure of the vapor bubble (61-62), the donor is ejected towards the receiver. There are many LIFT variations with different processes to transfer material, the original is the one already described, and it will be further discussed in this essay.

The Dynamic Release Layer LIFT (DRL-LIFT) is a technique used in delicate materials, which uses a sacrificial layer (dynamic release layer) added between the carrier and the donor. The laser is focalized in the DRL, which will induce pressure in the donor, causing it to be transferred to the receiver. This technique was proposed by Tolbert *et al*. (63)

The Matrix-Assisted Pulsed Laser Evaporation – Direct Write (MAPLE-DW) is a technique proposed by Piqué *et al*. (64) that combines the established MAPLE technique with LIFT. It limits the incident laser effect on the donor material. The matrix material is chosen to have a lower fusion temperature than the donor. The laser vaporizes the matrix, and the donor is released to the receiver.

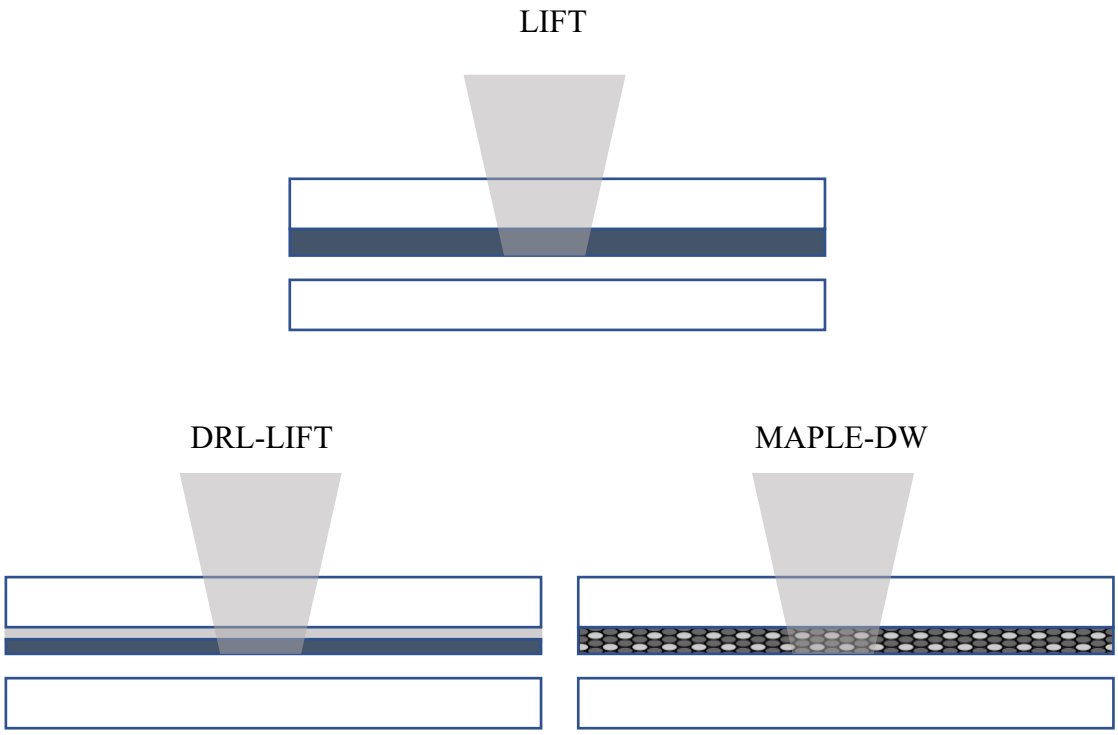

Figure 15 – LIFT techniques illustration.

Source: By the author.

3 EXPERIMENTAL

Chapter III addresses the experimental part of this project. It brings the experimental setup and material in detail and the methodology applied in order to achieve our results.

a) Experimental Setup

Two femtosecond laser systems were used to study the Platinum micromachining. The first one is a commercial Ti:Sapphire extended cavity femtosecond laser oscillator (Femtosource). The Femtosource system allows a combination of ultrashort pulses, centered at 800 nm, with pulse duration of about 50 fs and pulse energies around 100 nJ at a 5 MHz repetition rate, with an average power of 0,5 W.

The second system used is the Carbide laser, which has 216-fs pulses and fundamental wavelength centered at 1030 nm, second harmonic at 515 nm, and third harmonic at 343 nm. Carbide is based on a chirped pulse amplification (CPA) technique, using a diode-pumped Yb:KGW as the active medium. It also has a controlled repetition rate (1 MHz to ~100 Hz) via Pockels cell-based pulse selector. which allows one to select the number of incoming pulses.

The experimental setup uses the laser pulse to micromachine in Platinum samples. The light is guided by mirrors to a three-dimensional motorized translation stage, computer-controlled, with micrometric precision. The samples, composed of the Platinum thin film (donor) and glass (receiver), are placed, in contact, on the translation stage, while the laser beam is focalized in the sample's surface by a microscope objective (NA = 0.40). Above and aligned with the system, there is a CCD camera that allows monitoring of the process in real time. The computer-controlled translation stage enables to micromachine any form, like straight lines, circles, cubes, and so on. The setup system is illustrated in Fig. 7.

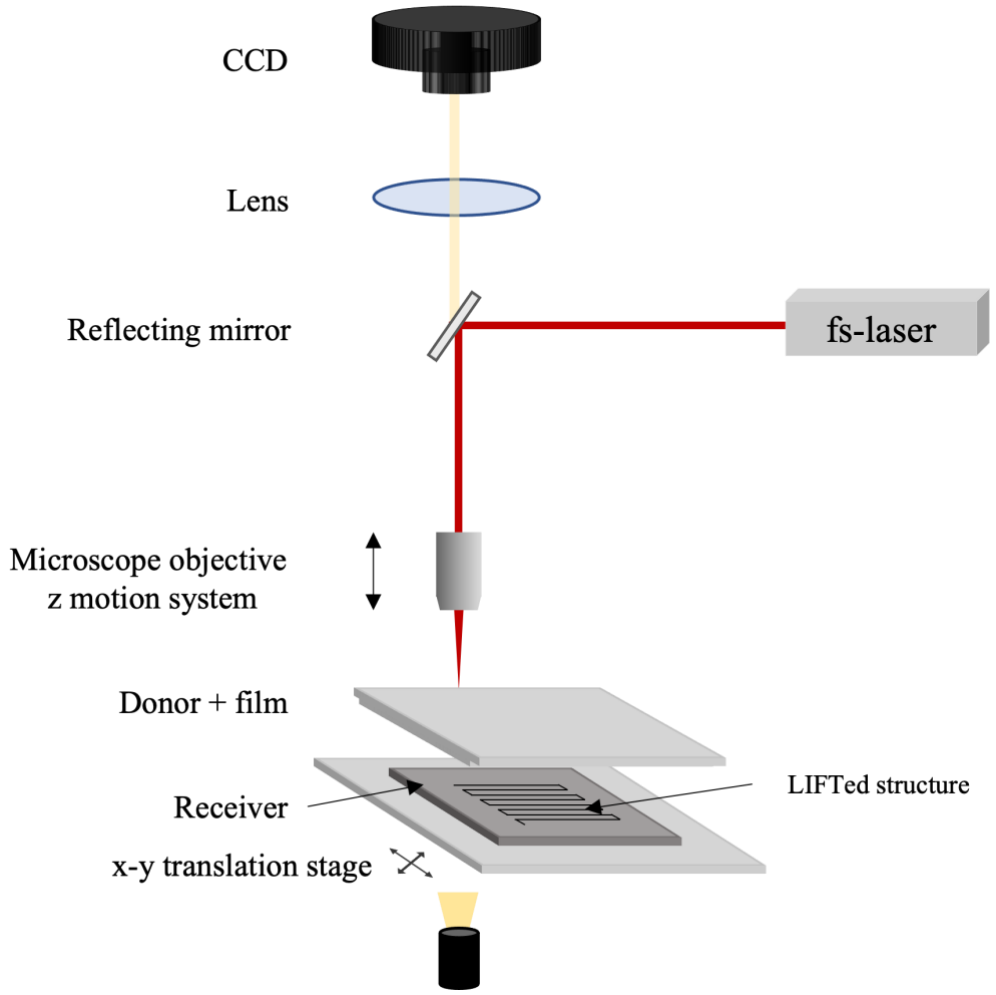

Figure 16 – Setup illustration.

Source: By the author.

b) Zero Damage Method

The zero damage method (32) was used to evaluate the incubation effect of the Platinum samples. This method uses Gaussian-intensity profiles with different energies to produce damage on the surface of the sample. The higher the energy applied, the larger will be the damage lines, as can be seen in Fig. 8.

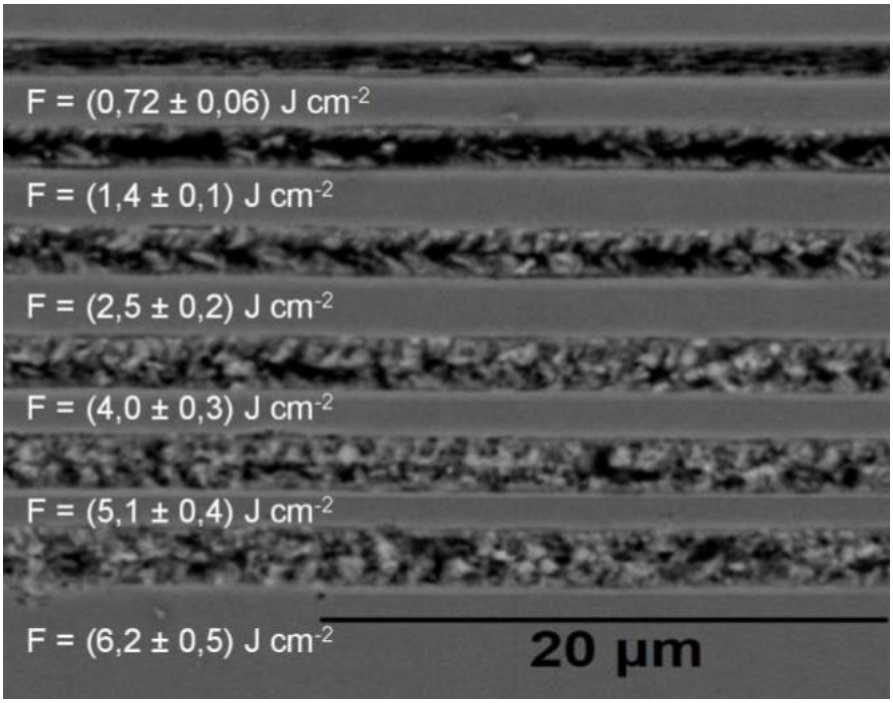

Figure 17 – SEM images of micromachined lines with different fluences on a GaN film.

Source: NOLASCO. (46)

Given the Gaussian-intensity spatial-temporal profile of the laser,

$$I(r,t) = I_0 \exp\left(-\frac{r^2}{\rho^2}\right)\exp\left(-\frac{t^2}{\tau^2}\right) \tag{3.1}$$

In which I_0 is the peak intensity, ρ and τ are the spatial and temporal radii at 1/e intensity. The pulse fluence can be calculated by integrating Eq. 3.1 in time, which gives,

$$F(r) = F_0 \exp\left(-\frac{r^2}{\rho^2}\right) \tag{3.2}$$

where $F_0 = \sqrt{\pi}\tau I_0$ is the peak fluence at the center of the beam. If this pulse is focused on a sample, it will generate a circular pattern with radius r_{th} and fluence F_{th}, given by Eq. 2.13, which can be described as,

$$r_{th}^2 = \left(\frac{w_0^2}{2}\right) ln\frac{E_p}{E_{th}} \tag{3.3}$$

where w_0^2 is the Gaussian beam waist at the focus region, E_p is the pulse energy and E_{th} is the threshold energy. The pulse energy is related to the peak fluence by,

$$E_p = F_0 \pi \rho^2 \tag{3.4}$$

The characterization of the fs-pulse damage on the material surface's is given by Eq. 3.3, and the threshold fluence (F_{th}) can be obtained by

$$F_{th} = \frac{2E_{th}}{\pi w_0^2} \tag{3.5}$$

c) Laser Induced Forward Transfer

Laser Induced Forward Transfer (LIFT) is a micromachining technique used to transfer material from one substrate (donor) to another (receiver), demonstrated by Bohandy (49) in 1986. This method can be used to transfer material in many kinds of materials, such as metals, polymers, and ceramics (65-67), focused on developing the quality and transferring more complex materials. (68-69) Figure 9 shows a copper deposition made by Bohandy in his LIFT demonstration paper.

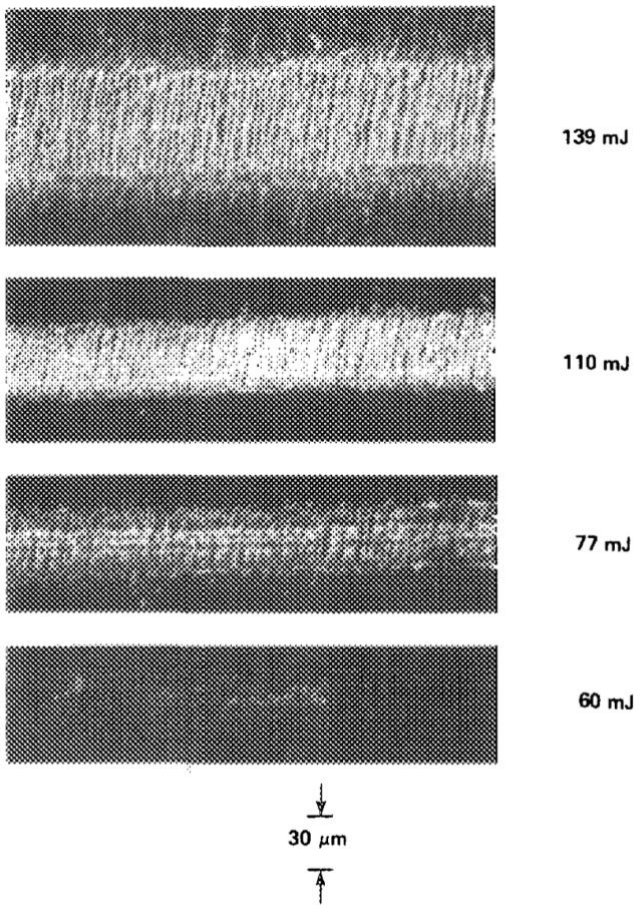

Figure 18 – Bohandy Cu deposition.

*Source: BOHANDY; KIM; ADRIAN.(*49)

LIFT is a high-resolution technique based on the ablation process. As can be seen in Fig. 10, a thin film (donor) is placed in contact with an uncoated substrate (receiver) in order to transfer nanoparticles. Focusing a high power and ultrashort laser beam in the backside of the donor, it creates a nonlinear ionization in its focal volume, generating a plasma, and then the ablation takes place. The pulse duration is shorter than the thermal dissipation around the focal volume, and because of it, the dissipation is confined in it.

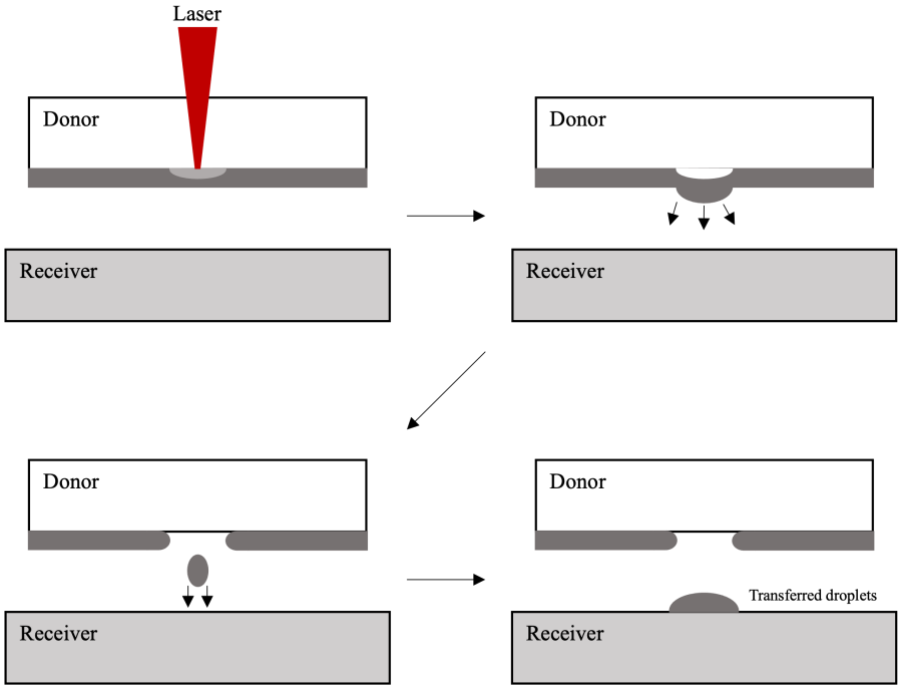

Figure 10 – Laser-Induced Forward Transfer illustration.

Source: By the author.

Depending on the applied laser energy to generate the ablation process, the material will be ejected in different ways, as demonstrated by P. Ralph. (70) For lower energies, the ejection has a cap-like format. As the energy increases, the ejection takes a jet-like format, and with even more energy, it takes a spray format, as seen in Fig. 11. Each ejection mechanism have an influence in how the droplets are deposited in the donor, and depending on this mechanism, satellite droplets can be seen, which can decrease the micromachine quality, making it difficult to analyze the transferred structures.

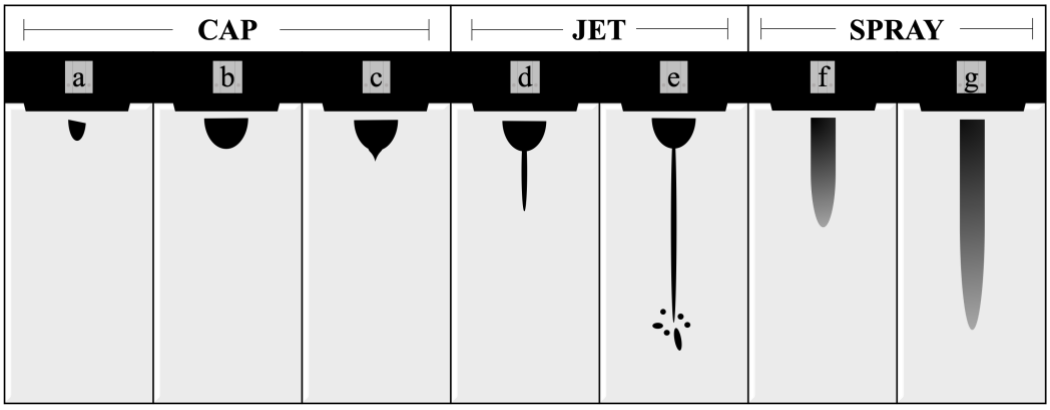

Figure 11 – Ejection illustration, with increasing energy from 'a' to 'g'.

Source: By the author.

Laser-Induced Forward Transfer is a versatile technique and can be used with different kinds of lasers. LIFT associated with a femtosecond (fs-LIFT) laser brings interesting advantages to the technique, as the thermal effects are reduced to the focal volume, the material is better preserved, and there is a higher spatial resolution. fs-LIFT also has some disadvantages compared with other lasers; for example, it implies difficulties to do larger-scale structures, and it is a more expensive technique.

d) Characterization techniques

Optical microscopy (Zeiss LSM 700) was used to obtain optical images of the lifted microstructures. In order to do a more detailed analysis, the micromachined samples were characterized by Atomic Force Microscopy (AFM) using Nanosurf's easyScan 2® and Scanning Electron Microscopy (SEM) with a FEI's Inspect F50 microscope. The sample's optical properties were analyzed by a UV-vis spectrophotometer (Shimadzu, UV-1800). To characterize the micromachined sample's surface, a profilometer (Nanovea, ST400, accuracy of 1 µm) was used.

4 RESULTS AND DISCUSSION

In this chapter, the goal is to report the experimental results of the femtosecond-pulse Platinum micromachining, and a comparison with the theoretical model, in order to validate the results and understand the femtosecond-laser processing technique.

The damage threshold fluence was determined for two laser systems, the Femtosource – with a wavelength of 800 nm, 5 MHz of repetition rate, and 80 fs pulse duration – and the Carbide – 1030 nm of wavelength, 216 fs pulse duration, and variable repetition rate, using the method described in previous sections.

The number of pulses per spot (N) was controlled by transferring platinum, via LIFT with different scanning speeds (v) and pulse repetition rate (f). It is calculated by taking the ratio between the summation of the intensities generated by fs-pulses in a single spot, and the intensity of a single pulse centered in that point. (71-72) This relation can be described as a Jacobi Theta function (73) (ϑ_3), given by,

$$N = \vartheta_3\left(0, e^{-2\left(\frac{V}{fw_0}\right)^2}\right) \tag{4.1}$$

For the case of a large amount of pulse superposition, the summation can be simplified, leading to

$$N = \sqrt{\frac{\pi}{2}}\frac{fw_0}{V} \approx 1.25\frac{fw_0}{V} \tag{4.2}$$

as the ratio $V/fw_0 \approx 0$, requiring a high repetition rate, or a very low scanning speed.

a) Femtosource

The Femtosource laser system, shown in Fig. 12, was the first one used to demonstrate the LIFT in Platinum. The LIFT method was performed with 10x, 20x, and 40x microscope objectives, that correspond to numerical aperture (NA) of 0.15, 0.40, and 0.65, respectively, focalizing the laser beam in the sample. For such laser system, the repetition rate was fixed at

5 MHz, scanning speeds of 10 and 20 µm/s were used. In order to transfer material from the donor to the receiver substrate, laser pulse energy was varied from 30 nJ to 58 nJ,

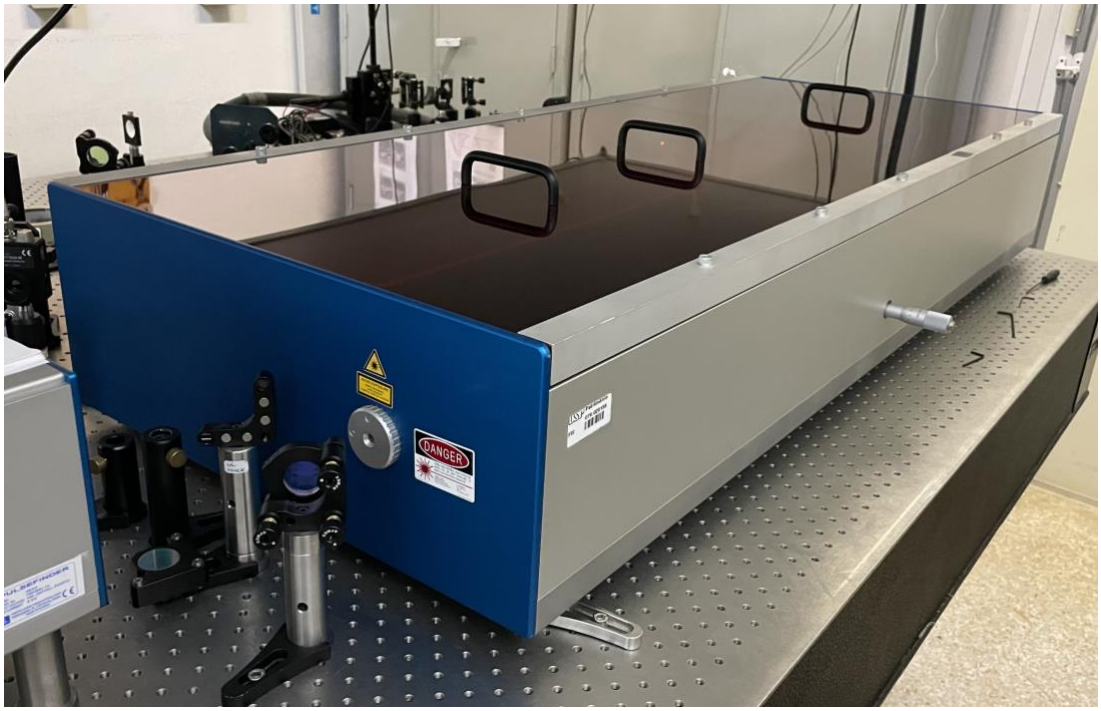

Figure 12 – Picture of the Laser Femtosource.

Source: By the author.

Groups of lines were deposited 40 µm apart for each transfer condition, and the depositions were analyzed in the optical microscope to determine the line-widths and to find the influence of the pulse energy and the scanning speed on the LIFT process. This procedure was used to determine the best conditions for micromachining and to calculate the threshold energy, as well as the threshold fluence.

In the depositions made with 0.40 NA objective and 10 µm/s of scanning speed, the laser pulse energy used were 32, 35, 41, 44, 50, and 58 nJ, respectively. The attempts to LIFT with the 0.15 and 0.65 NA objectives were unsuccessful. Using the 0.15 NA objective, there was insufficient energy to transfer material, as the focal area was too large. For the 0.65 NA objective, we were not able to transfer material, probably because the Platinum film was too thin, which made it difficult to find an optimum position to focalize the laser.

In the depositions made with 0.40 NA objective and 25 µm/s as scanning speed, the pulse energy employed were 31, 36, 40, 45, 50, and 57 nJ, respectively. For the same reasons as before, there were no depositions with the 0.15 and 0.65 NA objectives.

The lines width for each deposition was determined by an optical microscope. Figures 13a and 13b show some examples of the images taken in the microscope. In Fig. 13A, it is shown the deposition of lines transferred with 10 µm/s of scanning speed and 50 nJ. Figure 13B shows the deposition of lines transferred with 25 µm/s and 58 nJ of pulse energy.

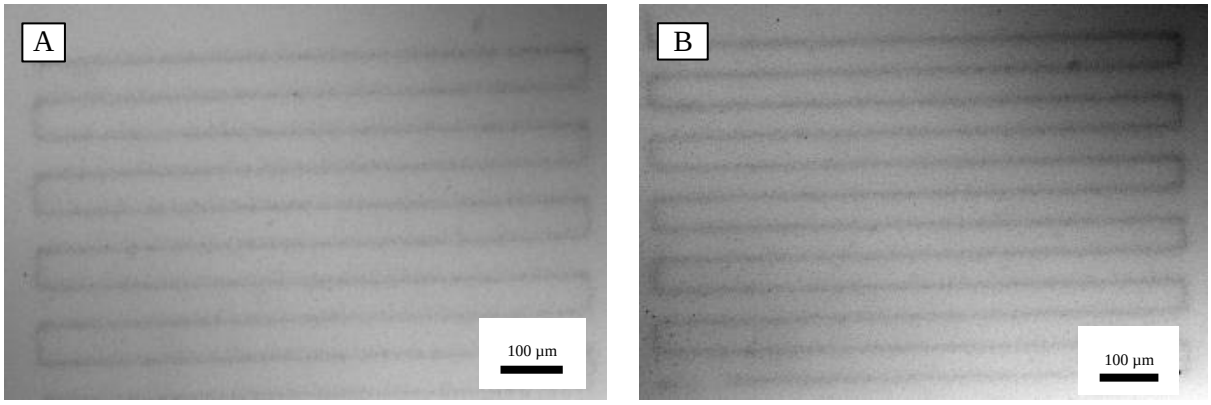

Figure 13 – Optical microscope images of LIFT obtained using (A) 10 µm/s and 250 mW and (B) 25 µm/s and 288 mW depositions.

Source: By the author.

For the procedure made with the 0.40 NA objective, 10 µm/s, and energies varying from 32 to 58 nJ, the line's width varied from 14 µm to 17 µm. For the transfers made with the 0.40 NA, 25 µm/s and energies varying from 31 to 57 nJ, the line's width varied from 15 µm to 17 µm. The transfer attempts for the lower energy was unsuccessful with 20 µm/s of scanning speed. The line's width were determined using an image software.

With the line's width measured from the optical microscope images, Eq. 3.3 can be used to calculate the threshold energy for each scanning speed. From a graph of the half of the line width (R) as a function of the pulse energy, the linear and angular coefficients obtained from the fitting line can be used to calculate the threshold energy, the threshold fluence, and number of pulses per spot using Eqs. 3.5 and 4.2, respectively.

For 5 MHz repetition rate and 10 µm/s scanning speed, the threshold energy calculated was 9.8 nJ, the threshold fluence $3\ x\ 10^{-3}\ J/cm^2$ and $9.3\ x\ 10^6$ pulses per spot. At 25 µm/s scanning speed, the threshold energy calculated was 19.8 nJ, the threshold fluence $6\ x\ 10^{-3}\ J/cm^2$ and $5.4\ x\ 10^6$ pulses per spot.

Figure 14 shows the square R as a function of the pulse energy, which is used to extract the threshold energy and fluence. The black line shows the 10 µm/s scanning speed depositions, whilst the grey one corresponds to the 25 µm/s scanning speed deposition.

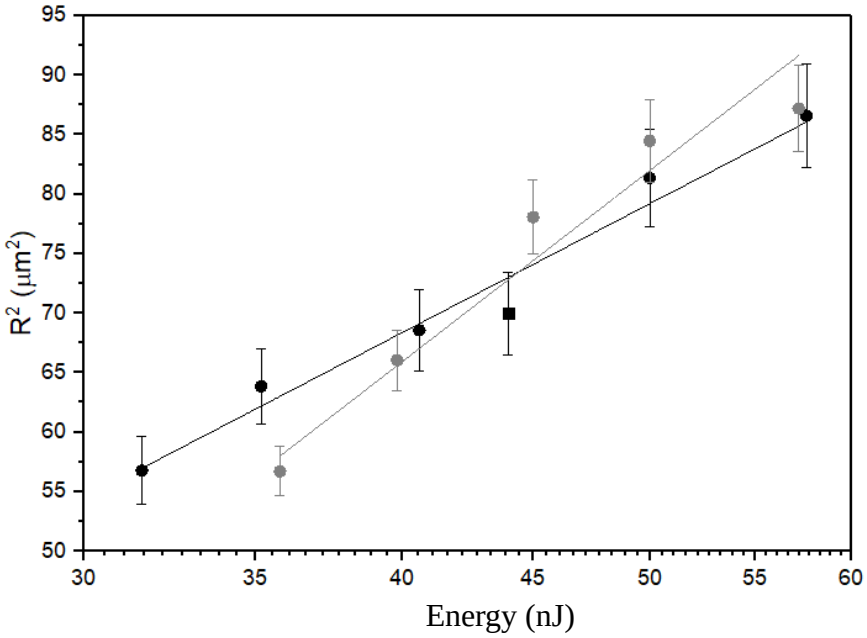

Figure 14 – Square radius in function of the pulse energy. Black line indicates the depositions for 10 µm/s scanning speed and the grey line for the 25 µm/s scanning speed.

Source: By the author.

b) Carbide

The second laser system used to perform LIFT with Pt was the Carbide (Figure 15). The LIFT was made with an optical objective of 10, 20, and 40 x, corresponding to numerical apertures of 0.15, 0.40, and 0.65, respectively, focalizing the laser beam in the sample. Such laser system allows variable repetition rate and output power at three wavelengths (343 nm, 515 nm, and 1030 nm). The continuously tunable repetition rate is adjustable from 60 kHz to 1MHz, combined with a built-in pulse picker for output pulse timing. It also has a minimum pulse duration of 216 fs (assuming a Gaussian pulse), adjustable in the range from 290 fs to 10 ps. All parameters are selected in the software.

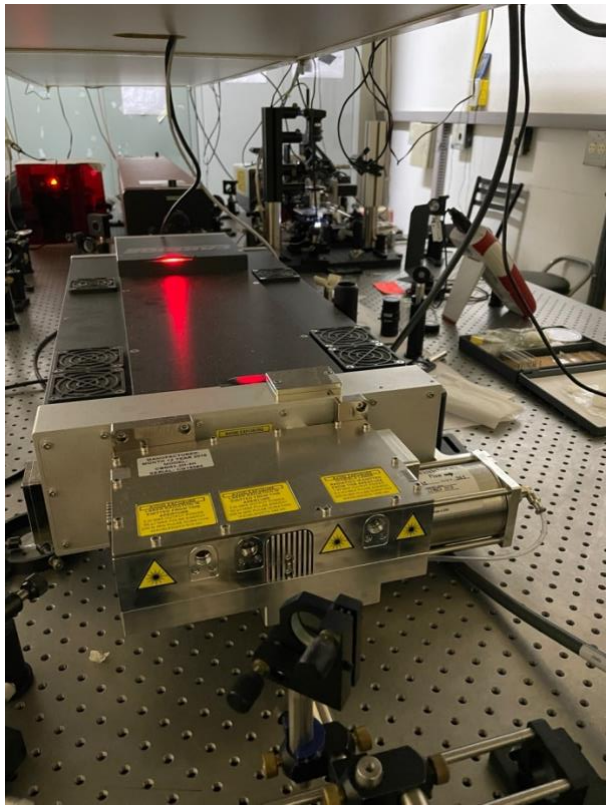

Figure 15 – Picture of the Laser Carbide.

Source: By the author.

i. Threshold energy characterization

The first step with the Carbide system was to identify the best conditions to realize the micromachining. Three repetition rates were selected to study; 1 kHz, 10 kHz, and 100 kHz, based on supplementary experiments. For each repetition rate, the depositions were made using 25 and 50 µm/s as scanning speeds.

Using the 0.40 NA objective, with 1 kHz and 25 µm/s, the laser pulse energies employed were 1.2, 2.2, 3.5, 5.1, 7.3, 9.9, 12.5 µJ, respectively. For 1 kHz and 50 µm/s, the laser pulse energies employed were 1.0, 2.2, 3.5, 4.6, 6.7, 9.0, and 15.0 µJ, respectively.

With the same objective as before, with 10 kHz and 25 µm/s, the laser pulse energies employed were 0.3, 0.4, 0.5, 0.6, 0.7, 0.8, 0.9, 1.0 µJ, respectively. For 10 kHz and 50 µm/s, the laser pulse energies employed were 0.2, 0.34, 0.5, 0., 0.7, 0.8, 0.9, and 1.0 µJ, respectively.

Figures 16 and 17 show optical microscope images of depositions made. Figure 16 shows a deposition of lines transferred with 1 kHz repetition rate, using (A) 50 µm/s and 9.0 µJ and (B) 25 µm/s and 9.9 µJ.

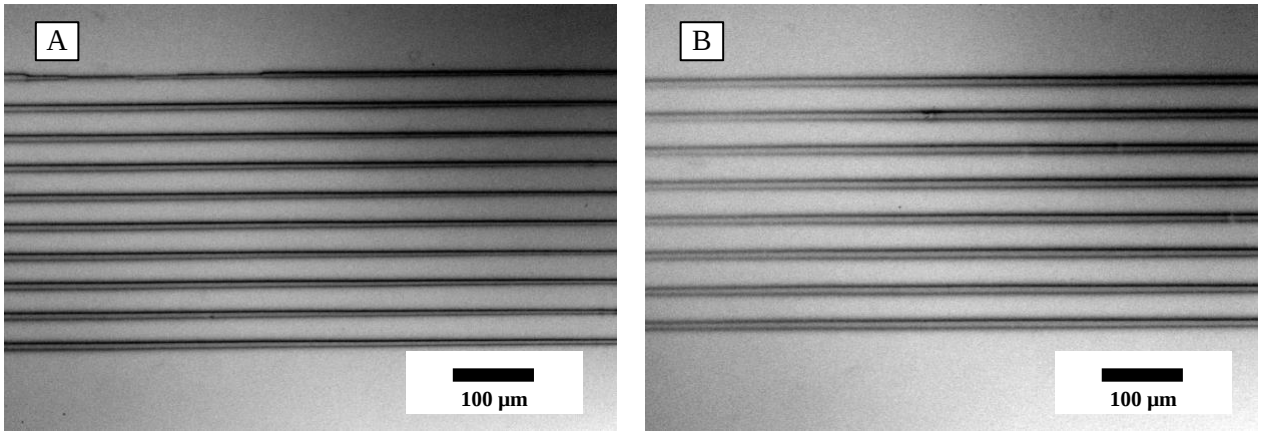

Figure 16 – Optical microscope images for LIFT made with (A) 1 kHz, 50 µm/s and 8.98 µJ and (B) 1 kHz, 35 µm/s and 9.86 µJ.

Source: By the author.

Figure 17 shows depositions of lines transferred with 10 kHz of repetition rate for (A) 25 µm/s and 0.6 µJ and (B) 50 µm/s and 0.7 µJ. As can be seen, the depositions made with this laser system are thicker and bulkier. Comparing Figs. 16 and 17, depositions made at 1 kHz are visually better.

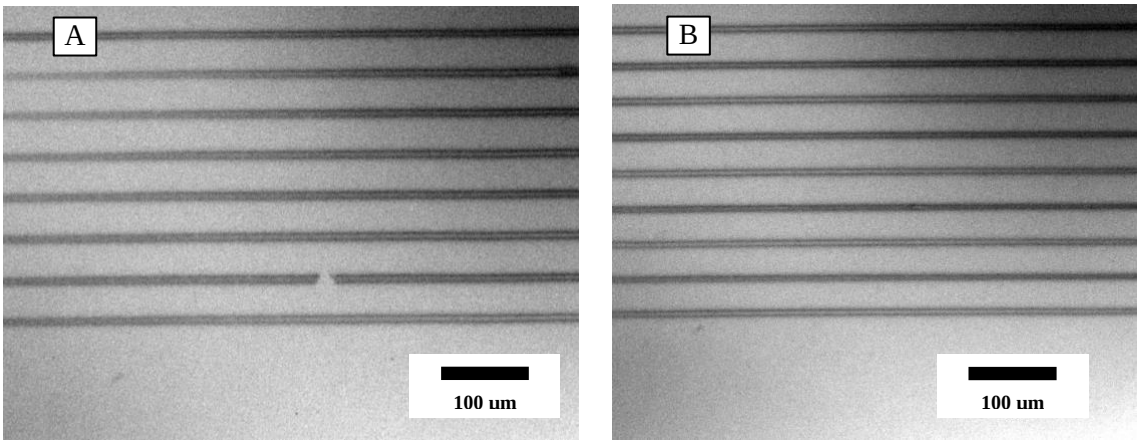

Figure 17 – Optical microscope images of LIFT obtained using (a) 10 kHz, 25 µm/s and 0.57µJ and (b) 10 kHz, 50 µm/s and 0.69 µJ

Source: By the author.

For the same reasons previously mentioned for the Femtosource laser system, attempts to produce LIFT with the Carbide system using 0.15 and 0.65 NA objectives were unsuccessful. Therefore, the 0.40 NA objective was chosen to continue the studies.

The same procedure was made using 100 and 200 kHz repetition rates and the same objective and scanning speeds. The energies used were from 36 nJ to 105 nJ for both speeds.

However, the obtained depositions' quality was poor (little amount of material and blurry images), making it impossible to analyze the data and calculate the threshold energy.

The same analyses presented before for the other laser system were performed here. For 1 kHz and 25 µm/s, with energies varying from 1 to 13 µJ, it resulted in depositions from 3.4 to 8.1 µm width. Using the same repetition rate and 50 µm/s, with energies varying from 1 to 15 µJ, the depositions widths ranged from 2.7 to 8.9 µm. Figure 18A shows the results obtained through the zero damage method.

For 1 kHz and 25 µm/s, the threshold energy obtained was 0.7 µJ, which corresponds to a fluence of $0.50\,J/cm^2$ (460 pulses per spot). At 50 µm/s of scanning speed, the threshold energy was 0.9 µJ (fluence $0.65\,J/cm^2$) for 230 pulses per spot.

The same method was used for 10 kHz and 25 µm/s, with energies varying from 0.25 to 1.00 µJ resulted in depositions widths from 4.2 to 7.4 µm. For 50 µm/s, with energies varying from 0.2 to 1.00 µJ, the depositions widths ranged from 4.7 to 7.6 µm. Figure 18B shows the results obtained through the zero damage method at kHz.

At a 10 kHz repetition rate and 25 µm/s of scanning speed, the threshold energy determined was 0.10 µJ, which corresponds to a threshold fluence $0.05\,J/cm^2$ 5570 pulses per spot. For 50 µm/s (2960 number of pulses per spot), the threshold energy determined was 0.20 µJ (threshold fluence $0.09\,J/cm^2$).

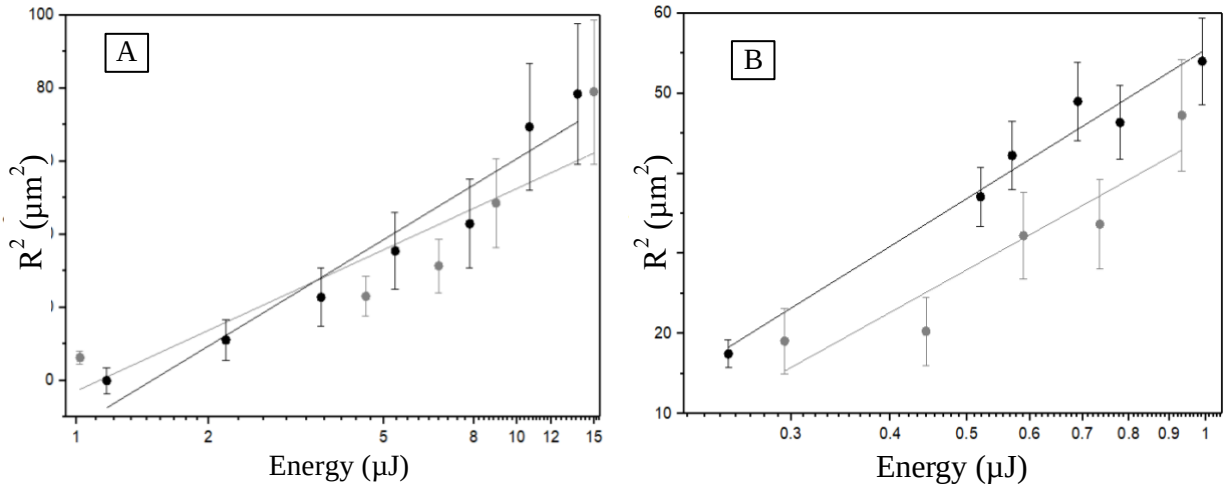

Figure 18 – Squared radius s a function of the pulse energy. The black line indicates the depositions for 25 µm/s scanning speed, and the grey line for the 50 µm/s scanning speed. Graphy (A) 1 kHz and (B) 10 kHz repetition rate.

Source: By the author.

Figure 19 displays a typical scanning electron microscopy (SEM) image of the Pt deposition achieved by LIFT, in which it can be observed that upon transferring Platinum nanoparticles (PtNP's) are observed in the receiver substrate.

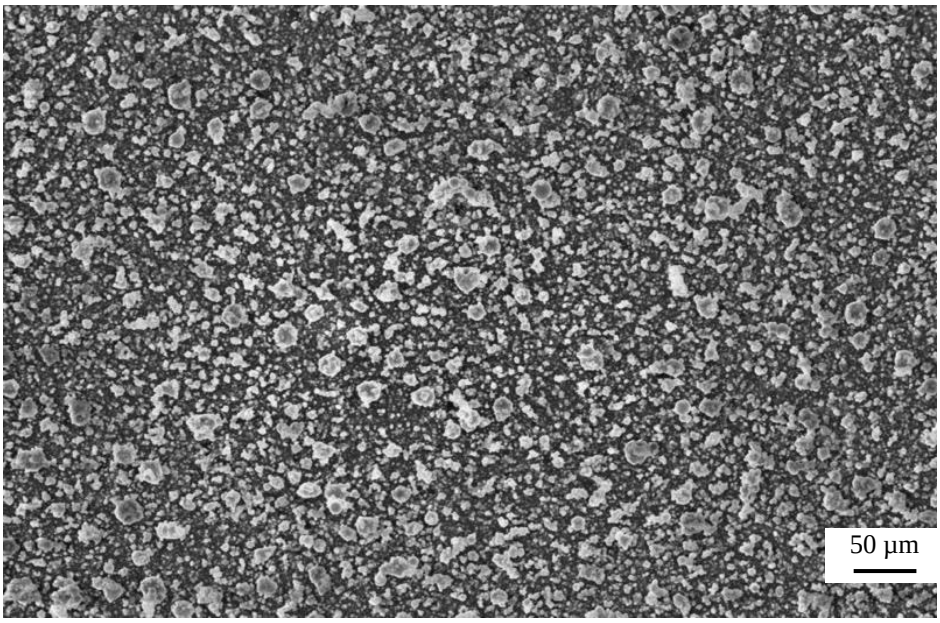

Figure 19 – SEM image of PtNP's in the LIFTed area. This deposition was carried out using 1 kHz repetition rate, 25 µm/s in Carbide's first harmonic (1030 nm).

Source: By the author.

From the results obtained using the Carbide laser system and analyzing the SEM and optical microscopy images, the optimum conditions to achieve LIFT Pt nanoparticles at 1030 nm are using a repetition rate of 1 kHz, scanning speed of 50 µm/s and pulse energy around 4 µJ.

ii. Incubation effect

The damage threshold fluence of platinum for a specific number of pulses (N) was determined using the Carbide laser system at 1030 nm. Using the method described before, with Eqs. 4.1 and 4.2, associated with the Zero Damage method (described in the Experimental), the threshold fluence was determined for N varying from 10 to 5500. To achieve such a number of pulses per spot (N), the laser repetition rate was varied from 300 Hz to 10 kHz, and the scanning speed from 25 µm/s to 370 µm/s. For each value of N, a graph of the radius squared as a function of the pulse energy was carried out in the same way as previously presented.

The incubation curve corresponds to the plot of the threshold fluence as a function of N, from which it is possible to study the effect of cumulative pulses on the LIFT. Many models have been proposed to describe the incubation effect(48,74), such as a simple empirical ansatz given by

$$F_{th,N} = F_1 N^{S-1} \tag{4.3}$$

where $F_{th,N}$ is the fluence for a pulse superposition *N*, F_1 is the fluence of a single pulse, and *S* is an incubation parameter. Another model considers the saturation of induced defects into account, which can be seen for a large number of pulses, and is described by

$$F_{th,N} = \left(F_{th,1} - F_{th,\infty}\right)e^{-k(N-1)} + F_{th,\infty} \tag{4.4}$$

where $F_{th,\infty}$ and $F_{th,1}$ are the infinite and single pulse threshold fluence, and *k* is an empirical constant (incubation parameter) that describes the efficiency of the cumulative effect; the higher its value, the fewer pulses are needed to reach the minimum damage threshold fluence ($F_{th,\infty}$), on the bottom plateau of an incubation effect curve.

In Fig. 19 it is presented the results of the incubation effect for the femtosecond micromachining of the Pt sample, using 216 fs pulses at 1030 nm wavelength. The dashed grey line corresponds to Eq. 4.4, correctly describing the experimental behavior of the $F_{th,N}$ saturation for the larger number of pulses per spot region. From this result, it can be observed a significant decrease in the threshold fluence from $(1{,}2 \pm 0{,}1)\ J/cm^2$ to a value of $(0{,}05 \pm 0{,}02)\ J/cm^2$ from 50 pulses per spot to 1000 pulses per spot. This behavior is described by the cumulative defects generated by the femtosecond pulses before the ablation process takes place. Increasing the number of pulses per spot interacting with the Pt thin film sample, the number of defects also increases, helping the optical damage process. This leads to a local electronic density modification, or creates of sub-bandgap energy levels, accelerating the ionization process.

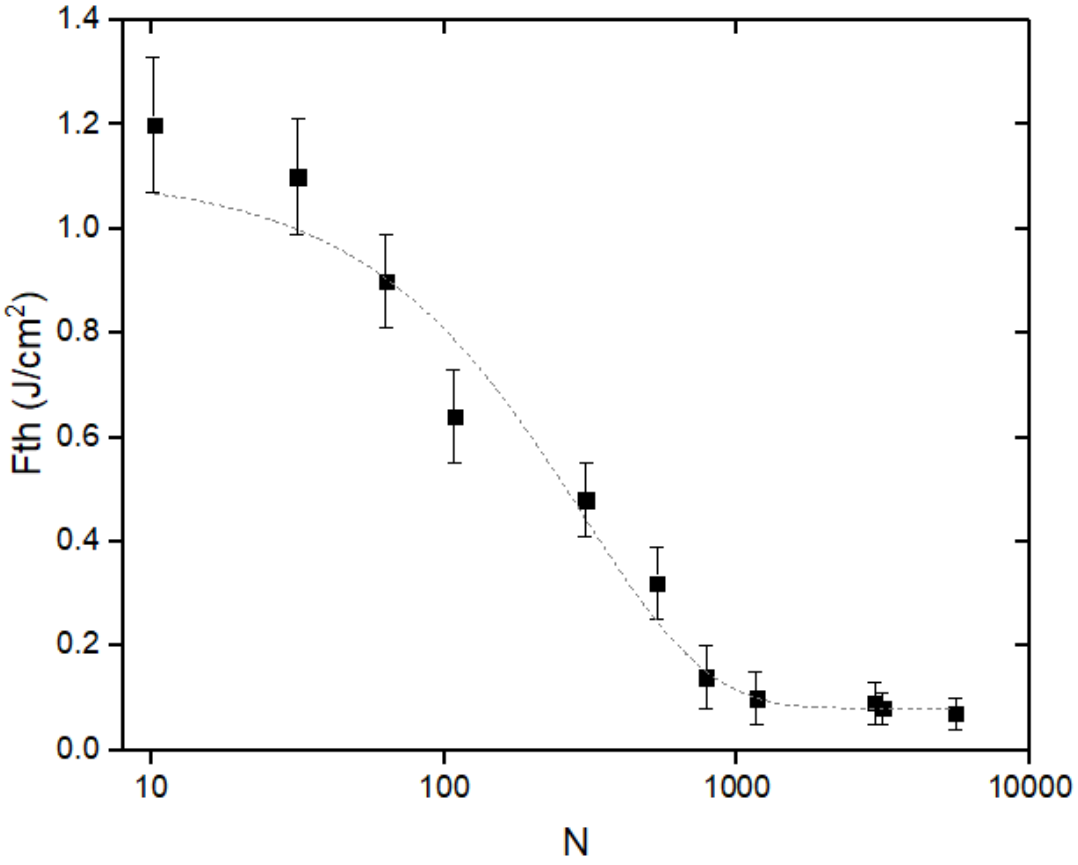

Figure 20 – Incubation effect, threshold fluence as a function of the number of pulses per spot. The graph was made using the calculations for depositions of N from 10 to 5500, varying the laser repetition rate from 300 Hz to 10 kHz and the scanning speed from 25 to 370 µm/s.

Source: By the author.

The same study was made using Carbide's second harmonic, at 515 nm. However, in this case, the energies were not enough to cause any damage to the platinum thin film. The second try was carried out using an objective with a higher numerical aperture to increase the intensity by focusing tightly on the laser beam. In this situation, however, given the small thickness of the film, we were not able to properly focus/position the sample in the z-axis, such that no LIFT was achieved.

iii. Grayscale

To demonstrate the capabilities of producing LIFT of platinum with different thicknesses, depositions were made in lines very close to each other, looking like a range of shades of gray, without an apparent color, called "grayscale". The procedure used to do it was to deposit lines very close to one another with the same laser condition. After a few lines were deposited, the laser's repetition rate was changed and the same number of were lines deposited

again, and so on. Changing the repetition rate changes the amount of material that can be transferred to the receiver film; performing such depositions with different conditions creates a grayscale palette. Figure 20 shows a micromachined greyscale, made in the following conditions: from bottom to top, 1 kHz repetition rate and 100 µm/s, 5 kHz and 100 µm/s, 10 kHz and 150 µm/s, 20 kHz and 200 µm/s, 50 kHz and 200 µm/s and finally 100 kHz and 200 µm/s. Clearly, the depositions in Fig. 20b on the top have less material LIFTed than the bottom ones, attesting that with lower repetition rates, the platinum depositions have a higher quality.

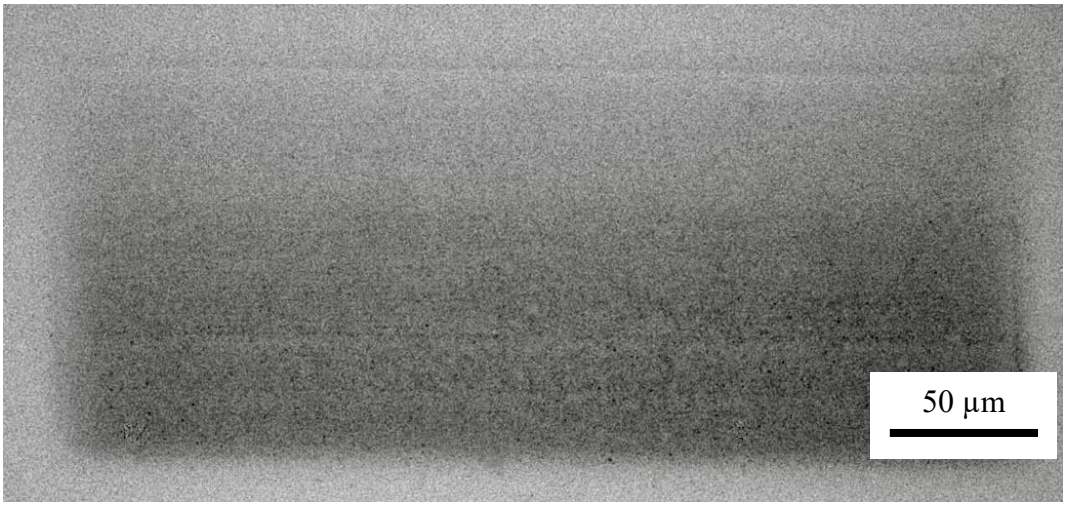

Figure 21 - Optical microscope image of the depositions made with different repetition rates and scanning speeds.

Source: By the author.

iv. 3D structure

To demonstrate the possibility of fabricating a tri-dimensional structure of planitum by LIFT, we used LIFT to produce a structure like the one illustrated in Fig. 21. LIFTed square areas were made one above another, each time smaller, creating a pyramid-like structure. The setup used was the same as before, but in this case, to be sure that the deposition film was in the correct place to make the layers, it was fixed in the translation stage, allowing to change the platinum film position to a not LIFTed area.

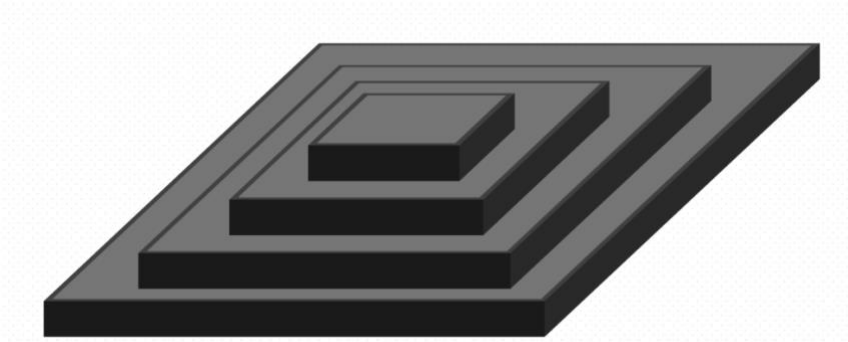

Figure 22 - Illustration of the pyramid-like structure, made by LIFTing different areas of Platinum one above another. Source: By the author.

The structure was made with three square layers, the base one with 300 μm^2, the middle one with 200 μm^2, and the top one with 100 μm^2. Figure 22 shows a top view SEM image of the micromachined structure. All the layers were made with the same conditions, 2 kHz repetition rate, 100 µm/s scanning speed and 3 µJ of pulse energy. The figure shows the possibility of making a tri-dimensional structure with the proposed technique.

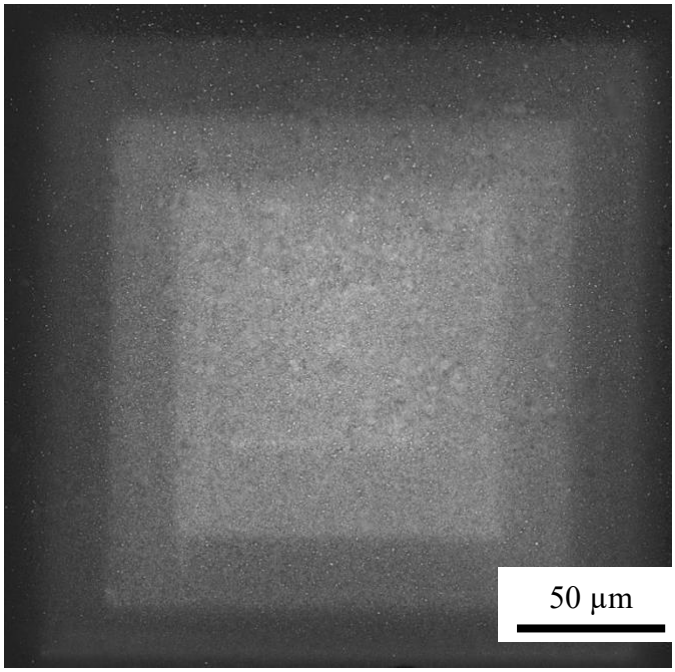

Figure 23 - LIFTed tri-dimensional structure SEM image, made with 2 kHz, 100 µm/s and 3 µJ conditions and three layers, with 300, 200 and 100 μm^s from bottom to top, respectively.

Source: By the author.

v PtNP's Conductivity

To measure the conductivity of the deposited platinum nanoparticles film, four layers of platinum were LIFTed in a 1 x 2.2 mm area in a film containing gold contacts, which were connected to a voltage source. The depositions were made in the optimum conditions, 2 kHz repetition rate, 100 µm/s scanning speed, and 3.5 µJ pulse energy. Measuring the current for different applied voltages, it was possible to calculate the resistivity and conductivity of the samples. The measurements were made by varying the voltage from -3 to 3 volts, and the currents found were from -2,52 to 2,25 nA. With a i x V linear graph, seen in Fig. 23, the linearization angular coefficient is the resistance, and with it, using the Eq. 4.5, the conductivity and resistivity are calculated.

The conductivity was calculated as 95.3 $\Omega.m$ and the resistivity as 0.01 S/m, concluding that the sample presents a very high resistivity. This result shows that, in order to use PtNP's for conductivity purposes, the depositions should have a higher quantity of material transferred, filling the empty spaces between the particles.

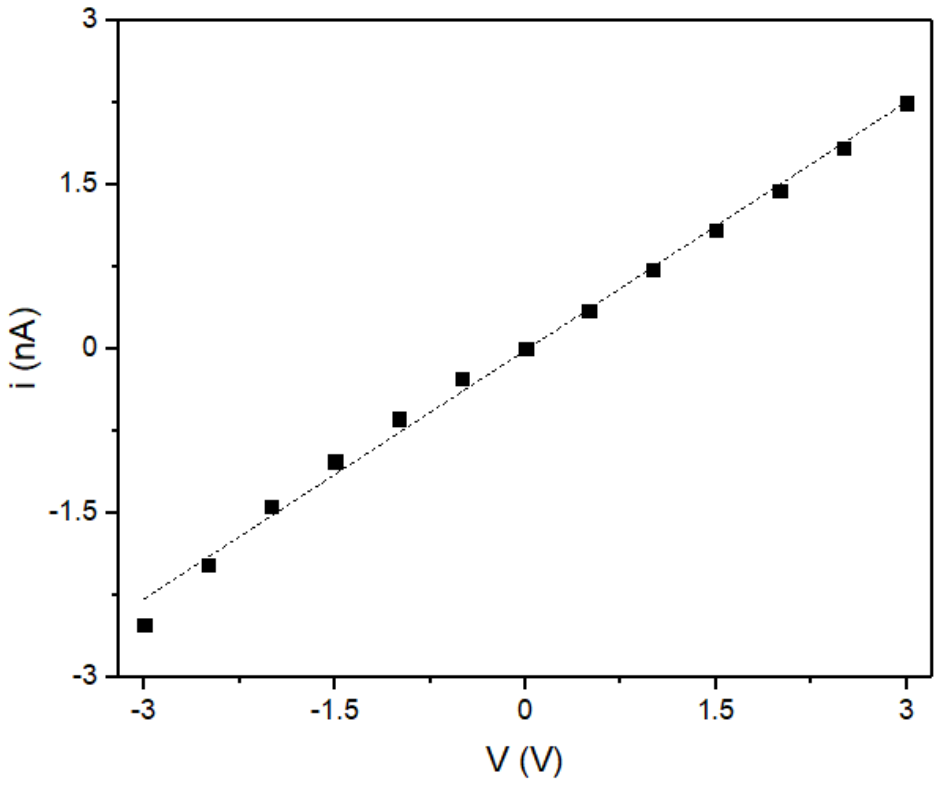

Figure 24 - Graph of current versus tension made to calculate the PtNP's resistivity.

Source: By the author.

5 CONCLUSIONS

In this dissertation, we have studied the fundamentals involved in the femtosecond laser-induced forward transfer of platinum at 1030, 800, and 515 nm using different laser systems. We used the zero damage method to calculate the damage threshold energies and fluences for different conditions. From the experimental data, we were able to study the incubation effect of platinum upon LIFT, by determining the threshold fluence as a function of the number of pulses per spot employed, in which the damage fluence decreases until it reaches a plateau of minimal fluence value.

The threshold energy and fluence were determined for two different laser systems; Femtosource and Carbide, and the optimum conditions to micromachine were found to be 9.8 nJ using 10 µm/s of scanning speed and repetition rate of 5 MHz, and 19.8 nJ using 25 µm/s scanning speed, which corresponds to depositions made with 9.4 x 10^6 pulses per spot and 5.4 x 10^6 pulses per spot, respectively. Carbide's deposition was performed by exploring a higher number of conditions, as the repetition rate is also variable for such laser. After many experiments with different repetition rates, scanning speeds, and pulse energies, the optimum conditions for LIFTing platinum nanoparticles were found to be in lower repetition rates (from 1 to 3 kHz), scanning speed in the range from 50 to 100 µm/s and using 3 to 5 µJ of laser energy, which corresponds to 250 to 400 pulses per spot. Such laser system allowed the deposition of better platinum structures by LIFT, as compared to the Femtosource.

To demonstrate the flexibility of the approach and understand the variations in the deposited material in different conditions, a "greyscale" structure was fabricated, showing that depending on the parameters used for LIFT, distinct thickness of platinum can be transferred in a controllable manner. Furthermore, LIFT was o used to fabricate tri-dimensional platinum structures. The structure was designed to be a pyramid-like structure, with different areas of PtNP's deposited one on top of the other. The SEM images of the structure showed the viability of micromachining a tri-dimensional structure, opening paths to incoming technology research.

In conclusion, this study work studied the femtosecond laser-induced forward transfer of platinum, determining the optimum conditions for depositing platinum nanoparticles using two different laser systems. The influence of repetition rate in the transferred material was shown, and the viability of building a tri-dimensional structure was demonstrated. Besides what we accomplished in this dissertation, we look forward to analyzing different applications of the femtosecond micromachining of platinum and other materials.

REFERENCES

1 MAIMAN, T. H. Stimulated optical emission in ruby. *Nature*, v. 187, n.4736, p. 493-494,1960.

2 LIU, X.; DU, D.; G. MOUROU, G. Laser ablation and micromachining with ultrashort laser pulses. *IEEE Journal of Quantum Electronics*, v. 33, n. 10, p. 1706–1716, 1997.

3 CHICHCOV, B. N. *et al*. Femtosecond, picosecond and nanosecond laser ablation of solids. *Applied Physics A*: materials science & processing, v. 63, n. 2, p. 109-115,1996.

4 BARRON, J. A. *et al*. Biological laser printing: a novel technique for creating heterogeneous 3-dimensional cell patterns. *Biomedical Microdevices*, v. 6, n. 2, p. 139–147, 2004.

5 CHIA H. N.; WU, B. M. Recent advances in 3D printing of biomaterials. *Journal of Biological Engineering*, v. 9, n. 4, p. 1–14, 2015.

6 BUSCH, K.; SOUKOULIS, C. M. Direct laser writing of three-dimensional photonic-crystal templates for telecommunications. *Nature Materials*, v. 3, n. 7, p. 444–447, 2004.

7 KRÜGER, J.; KAUTEK, W. Ultrashort pulse laser interaction with dielectrics and polymers. *Advances in Polymer Science*, v. 168, p. 247–289, 2004. DOI:10.1007/b12683.

8 SAMAD, R. E. *et al*. Ultrashort laser pulses machining. *In*: PESHKO, I. (ed.). *Laser pulses* - theory, technology, and applications. London: InTech, 2012. DOI: 10.5772/46235.

9 ESROM, H. *et al*. New approach of a laser-induced forward transfer for deposition of patterned thin metal films. *Applied Surface Science*, v. 86, n. 1-4, p. 202–207, 1995.

10 KUZNETSOV, A. I. *et al*. Laser-induced jet formation and droplet ejection from thin metal films. *Applied Physics A*, v. 106, p. 479–487, 2012. DOI: 10.1007/s00339-011-6747-8.

11 DELAPORTE, P. *et al*. Applications of laser printing for organic electronics. *Proceedings of SPIE*, v. 8607, 2013. DOI: 10.1117/12.2004062.

12 RAPP, C. *et al*. Improvement in semiconductor laser printing using a sacrificial protecting layer for organic thin-film transistors fabrication. *Applied Surface Science*, v. 257, n. 12, p. 5245–5249, 2001.

13 LI, G. *et al*. 3D printed graphene/nickel electrodes for high areal capacitance electrochemical storage. *Journal of Materials Chemistry A*. v. 7, n. 8, p. 4055–4062, 2019.

14 FERNANDEZ-PRADAS, J. M. *et al*. Laser-induced forward transfer of biomolecules. *Thin Solid Films*, v. 453–454, p. 27–30, 2004.

15 ARNOLD, C.; SERRA, P.; PUQUE, A. Laser direct-written techniques for printing of complex materials. *MRS Bulletin*, v. 32, p. 23–31, 2007. DOI: 10.1557/mrs2007.11.

16 SANZ, M. *et al*. Femtosecond laser deposition of TiO2by laser induced forward transfer. *Thin Solid Films*, v. 518, N. 19, p. 5525–5529, 2010.

17 EVANOFF, D. D.; CHUMANOV, G. Synthesis and optical properties of silver nanoparticles and arrays. *ChemPhysChem*, v. 6, n. 7, p. 1221–1231, 2005.

18 HUNG, J. H. *et al*. Metal nanoparticle generation using a small ceramic heater with a localheating area. *Journal of Aerosol Science*, v. 37, n. 12, p. 1662–1670, 2006.

19 XIA Y.; SUN, Y. Shape-controlled synthesis of gold and silver nanoparticles. *Science*, v. 298, n. 5601, p. 2176–2179, 2002.

20 CREIGHTON, J. A.; EADON, D. G. Ultraviolet–visible absorption spectra of the colloidal metallic elements. *Journal of the Chemical Society, Faraday Transactions*, v. 87, n. 24, 1991. DOI: 10.1039/FT9918703881.

21 SHAO-HORN, Y. *et al*. Instability of supported platinum nanoparticles in low-temperature fuel cells. *Topics in Catalysis*, v. 46, n. 3–4, Dec. 2007. DOI: 10.1007/s11244-007-9000-0.

22 FERREIRA, P. J. *et al*. Instability of Pt/C electrocatalysts in proton exchange membrane fuel cells. *Journal of the Electrochemical Society*, v. 152, n. 11, 2005. DOI: 10.1149/1.2050347.

23 CHOI, Y.-J. *et al*. Fabrication and characterization of direct-patternable ZnO films containing Pt nanoparticles. *Japanese Journal of Applied Physics*, v. 48, n. 3, Mar. 2009. DOI: 10.1143/JJAP.48.035504.

24 DAVIS, T. L. The discovery of the elements (Weeks, Mary Elvira). *Journal of Chemical Education*, v. 10, n. 11, Nov. 1933. DOI: 10.1021/ed010p710.1.

25 MURATA, K. Spectrochemical analysis for trace elements in geological materials. *In*: SYMPOSIUM ON SPECTROCHEMICAL ANALYSIS FOR TRACE ELEMENTS, 60., 1957, Atlantic City. *Proceedings*. […] Atlantic City: ASTM, 1958. DOI: 10.1520/STP39566S.

26 GUPTA, S. V. Meter convention and evolution of base units. *In*: GUPTA, S. V. *Units of measurement*. Cham: Springer, 2020. p. 97-118. (Springer series in material science, v. 122).

27 BORGHAEI, H. *et al*. Nivolumab versus docetaxel in advanced nonsquamous non–small-cell lung cancer. *New England Journal of Medicine*, v. 373, n. 17, Oct. 2015. DOI: 10.1056/NEJMoa1507643.

28 GASTEIGER, H. A. *et al*. Activity benchmarks and requirements for Pt, Pt-alloy, and non-Pt oxygen reduction catalysts for PEMFCs. *Applied Catalysis B*, v. 56, n. 1–2, Mar. 2005. DOI: 10.1016/j.apcatb.2004.06.021.

29 XU, X. Single-junction polymer solar cells with 16.35% efficiency enabled by a platinum(II) Complexation Strategy. *Advanced Materials*, v. 31, n. 29, July 2019. DOI: 10.1002/adma.201901872.

30 GENÇ, E. *et al*. Production and characterization of titanium (Ti), platinum (Pt) and tantalum (Ta) thin films for native DNA biosensors. *AIP Conference Proceedings*, v. 1815, n. 1, 2017. DOI: 10.1063/1.4976460.

31 LIU, C. *et al*. A hot platinum thin film anemometer. In: INTERNATIONAL CONFERENCE ON ELECTRONIC PACKAGING TECHNOLOGY & HIGH DENSITY PACKAGING, 11., 2010, Xi'an. *Proceedings* […] Xi'an: IEEE, Aug. 2010. DOI: 10.1109/ICEPT.2010.5582792.

32 LIU, J. M. Simple technique for measurements of pulsed gaussian-beam spot sizes. *Optics Letters*, v. 7, n. 5, p. 196–198, 1982.

33 BOYD, R. W. *The nonlinear optical susceptibility*. Burlington: Academic Press, 2008.

34 Franken, P. A. *et al*. Generation of optical harmonics. *PhysicalReview Letters*, v. 7, n. 4, Aug. 1961, DOI: 10.1103/PhysRevLett.7.118.

35 AMS, M. *et al*. Investigation of ultrafast laser--photonic material interactions: challenges for directly written glass photonics. *IEEE Journal of Selected Topics in Quantum Electronics*, v. 14, n. 5, 2008. DOI: 10.1109/JSTQE.2008.925809.

36 KELDYSH, L. V. Ionization in the field of a strong electromagnetic wave. *Soviet Physics JETP*, v. 20, 1965.

37 IPPEN, E. P. Principles of passive mode locking. *Applied Physics B*: laser and optics, v. 58, p. 159–170, 1994.

38 RAPOPORT W. R.; KHATTAK, C. P. Titanium sapphire laser characteristics. *Applied Optics*, v. 27, n. 13, p. 2677–2684, 1988.

39 FOWLES, G. R. *Introduction to modern optics*. New York: Dover Publications, 1975.

40 ALMEIDA, G. F. B. *Femtosecond laser writing of nonlinear waveguides in Gorilla® glass and L-threonine organic crystals*. 2018. Tese (Doutorado em Ciências) – Instituto

de Física de São Carlos, Universidade de São Paulo, São Carlos, 2018. DOI: 10.11606/T.76.2018.tde-04062018-152453.

41 HERCHER, M. Laser induced damage in transparent media. *Journal of the Optical Society of America*, v. 54, n. 2, p. 563, 1964.

42 PRONKO, P. P. *et al*. Machining of submicron holes using a femtosecond laser at 800-nm. *Optical Communications*, v. 14, n. 1–2, p. 106–110, 1995.

43 ANISIMOV, S.; KAPELIOVICH, B. L.; PERELMAN, T. Electron emission from metal surfaces exposed to ultrashort laser pulses. *Zhurnal Eksperimentalnoi I Teoreticheskoi Fiziki*, v. 66, p. 776–781, 1974.

44 D. PEREZ, D.; LEWIS, L. J. Molecular-dynamics study of ablation of solids under femtosecond laser pulses. *Physical Review B*, v. 67, n. 18, p. 184102, 2003.

45 P. LORAZO, P.; LEWIS, L. J.; MEUNIER, M. Short-pulse laser ablation of solids: from phase explosion to fragmentation. *Physical Review Letters*, v. 91, n. 22, p. 225502, 2003.

46 NOLASCO, L. K. *Investigation of the fs-micromachining process in GaN and diamond*. 2021. Dissertation (Master in Science) – Escola de Engenharia de São Carlos, Universidade de São Paulo, São Carlos, 2021. DOI: 10.11606/D.18.2021.tde-22042021-165900.

47 MERO, M. On the damage behavior of dielectric films when illuminated with multiple femtosecond laser pulses. *Optical Engineering*, v. 44, n. 5, p. 051107, 2005.

48 ASHKENASI, D.; LORENZ, M.; STOIAN, R.; ROSENFELD, A. Surface damage threshold and structuring of dielectrics using femtosecond laser pulses: the role of incubation. *Applied Surface Science*, v. 150, n. 1, p. 101–106, 1999.

49 BOHANDY, J.; KIM, B. F.; ADRIAN, F. J. Metal deposition from a supported metal film using an excimer laser. *Journal Applied Physics*, v. 60, n. 4, p. 1538–1539, 1986. DOI: 10.1063/1.337287.

50 ADRIAN, F. J. A study of the mechanism of metal deposition by the laser-induced forward transfer process. *Journal of Vacuum Science & Technology B*: microelectronics and nanometer structures, v. 5, n. 5, p. 1490, Sept. 1987. DOI: 10.1116/1.583661.

51 PIQUÉ, A.; SERRA, P. *Laser printing of functional materials*: 3D microfabrication, electronics and biomedicine. New York: John Wiley & Sons, 2018.

52 FOGARASSY, E. *et al*. Laser- induced forward transfer of high-Tc YBaCuO and BiSrCaCuO superconducting thin films. *Journal of Applied Physics*, v. 66, n. 1, p. 457–459, 1989.

53 NARAZAKI, A. *et al*. Nano- and microdot array formation of FeSi2 by nanosecond excimer laser-induced forward transfer. *Applied Physics Express*, v. 1, n. 5, p. 057001, 2008.

54 YANG, L. *et al*. Microdroplet deposition of copper film by femtosecond laser-induced forward transfer. *Applied Physics Letters*, v. 89, n. 16, p. 161110, 2006.

55 BOHANDY, J.; KIM, B. F.; ADRIAN, F. J. Metal deposition from a supported metal film using an excimer laser. *Journal of Applied Physics*, v. 60, n. 4, p. 1538–1539, 1986.

56 MOGYORÓSI, P. *et al*. Pulsed laser ablative deposition of thin metal films. *Applied Surface Science*, v. 36, n. 1-4, p. 157–163, 1989.

57 TÓTH, Z.; SZÖRÉNYI, T.; TÓTH, A. L. Ar+ laser-induced forward transfer (lift): a novel method for micrometer-size surface patterning. *Applied Surface Science*, v. 69, n. 1-4, p. 317–320, 1993.

58 ESROM, H. *et al*. New approach of a laser-induced forward transfer for deposition of patterned thin metal films. *Applied Surface Science*, v. 86, n. 1-4, p. 202–207, 1995.

59 ZHOU, Z.; MA, W. Investigation of thermomechanical responses in ultrafast laser heating of metal nanofilms. *Thin Solid Films*, v. 519, n. 22, p. 7940–7946, 2011.

60 SHUGAEV, M. V.; BULGAKOVA, N. M. Thermodynamic and stress analysis of laser-induced forward transfer of metals. *Applied Physics A*, v. 101, p. 103–109, 2010. DOI: 10.1007/s00339-010-5767-0.

61 RÖDER, T. C.; KÖHLER, J. R. Physical model for the laser induced forward transfer process. *Applied Physics Letters*, v. 100, n. 7, p. 071603, 2012.

62 VEIKO, V. P. *et al*. Laser induced film deposition by lift physical mechanisms and applications. *Laser and Particle Beams*, v. 24, n. 2, p. 203–209, 2009.

63 TOLBERT, W. A. *et al*. High-speed color imaging by laser ablation transfer with a dynamic release layer: fundamental mechanisms. *Journal of Imaging Science*, v. 37, n. 4, p. 411–421, 1993.

64 PIQUÉ, A. *et al*. A novel laser transfer process for direct writing of electronic and sensor materials. *Applied Physics A*, v. 69, Suppl. 1, p. S279–S284, 1999.

65 TOLBERT, W. A. *et al*. High-speed color imaging by laser ablation transfer with a dynamic release layer: fundamental mechanisms. *Journal of Imaging Science*, v. 37, n. 4, p. 411–421, 1993.

66 BLANCHET, G. B. *et al*. Large area, high resolution, dry printing of conducting polymers for organic electronics. *Applied Physics Letters*, v. 82, n. 3, p. 463–465, Jan. 2003. DOI: 10.1063/1.1533110.

67 PIQUÉ, A. *et al*. A novel laser transfer process for direct writing of electronic and sensor materials. *Applied Physics A*, v. 69, n. 7, p. S279–S284, 1999. DOI: 10.1007/s003390051400.

68 CHIA H. N.; WU, B. M. Recent advances in 3D printing of biomaterials. *Journal of Biological Engineering*, v. 9, n. 1, p. 4, Dec. 2015. DOI: 10.1186/s13036-015-0001-4.

69 ARNOLD, C. B.; SERRA, P.; PIQUÉ, A. Laser direct-write techniques for printing of complex materials. *MRS Bulletin*, v. 32, n. 1, p. 23–31, Jan. 2007. DOI: 10.1557/mrs2007.11.

70 POHL, R. *Laser-induced forward transfer of pure metals*. 2015. Dissertation (Applied Laser Technology) - Faculty of Engineering Technology, University of Twente, Enschede, 2015. DOI: 10.3990/1.9789036538695.

71 ALMEIDA, G. F. B. *et al*. Incubation effect during laser micromachining of GaN films with femtosecond pulses. *Journal of Material Science*: materials in electronics, v. 30, p. 16821–16826, 2019.

72 MACHADO, L. M. *et al*. D-Scan measurement of ablation threshold incubation effects for ultrashort laser pulses. *Optics Express*, v. 20, p. 1287–1301, 2012.

73 OWEN, D. B.; ABRAMOWITZ, M.; STEGAN, I. A. Handbook of mathematical functions with formulas, graphs, and mathematical tables. *Technometrics*, v. 7, p. 78, 1965.

74 SUN, Z.; LENZNER, M.; RUDOLPH, W. Generic incubation law for laser damage and ablation thresholds. *Journal of Applied Physics*, v. 117, n. 7, p. 073102, Feb. 2015. DOI: 10.1063/1.4913282.